

Modeling Approach for Evaluating Radionuclide Transport in Nuclear-Stimulated Gas Reservoirs

prepared by

Clay Cooper and Jenny Chapman

submitted to

Nevada Operations Office
National Nuclear Security Administration
U.S. Department of Energy
Las Vegas, Nevada

SEPTEMBER 2001

Publication No. 45186

Reference herein to any specific commercial product, process, or service by trade name, trademark, manufacturer, or otherwise, does not necessarily constitute or imply its endorsement, recommendation, or favoring by the United States Government or any agency thereof or its contractors or subcontractors. The views and opinions of authors expressed herein do not necessarily state or reflect those of the United States Government or any agency thereof.

This report has been reproduced directly from the best available copy.

Available for sale to the public, in paper, from:

U.S. Department of Commerce
National Technical Information Service
5285 Port Royal Rd.
Springfield, VA 22161
phone: 800.553.6847
fax: 703.605.6000
email: order@ntis.fedworld.gov
online ordering: <http://www.ntis.gov/ordering.htm>

Available electronically at <http://www.doe.gov/bridge>

Available for a processing fee to the U.S. Department of Energy and its contractors, in paper, from:

U.S. Department of Energy
Office of Scientific and Technical Information
P.O. Box 62
Oak Ridge, TN 37831-0062
phone: 423.576.8401
fax: 423.576.5728
email: reports@adonis.osti.gov

Modeling Approach for Evaluating Radionuclide Transport in Nuclear-Stimulated Gas Reservoirs

Prepared by

Clay Cooper and Jenny Chapman
Division of Hydrologic Sciences
Desert Research Institute
University and Community College System of Nevada

Publication No. 45186

Submitted to

Nevada Operations Office
National Nuclear Security Administration
U.S. Department of Energy
Las Vegas, Nevada

September 2001

The work upon which this report is based was supported by the U.S. Department of Energy under Contract #DE-AC08-00NV13609. Approved for public release; further dissemination unlimited.

ABSTRACT

The U.S. Department of Energy (DOE) is operating an environmental restoration program to characterize, remediate, and close non-Nevada Test Site locations where nuclear devices were detonated. Three of these sites -- Project Rio Blanco and Project Rulison in western Colorado, and Project Gasbuggy in northwest New Mexico -- were the location of low-permeability gas reservoirs that had been stimulated with nuclear devices to induce secondary fracture permeability. An approach to the evaluation of radionuclide transport in those gas reservoirs was developed around numerical analysis.

A conceptual model is presented here where the two-phase flow of gas and liquid occurs under structurally controlled pressure gradients on the order of 10 MPa per km. Radionuclide transport occurs in both the liquid and gas phases, and is able to partition between phases based upon Henry's law. Flow is modeled assuming a multiphase form of Darcy's law, with retardation occurring as radionuclide decay and matrix diffusion. Our approach is to develop the model heuristically, that is, to first present the results of simple two-dimensional simulations and then to include more complexity. Using properties at the Rio Blanco site as an example, simulations were run assuming with homogeneous permeability on the order of $3 \times 10^{-17} \text{ m}^2$. These simulations suggest that radionuclide transport is contained within 250 m of the cavity/chimney for 100 years after the detonations. A more complex model is developed that incorporates discrete fractures throughout the porous matrix. Our analysis shows qualitative changes in transport behavior but quantitatively the radionuclide transport field is similar to that of the porous media simulations.

Not surprisingly, the results suggest sensitivity to fracture hydraulic properties, which are largely unknown. Further analysis is required to accurately assess various fracture models and their uncertainty on the large-scale transport of radionuclides in the reservoirs.

CONTENTS

ABSTRACT.....	ii
LIST OF FIGURES	iv
LIST OF TABLES.....	iv
LIST OF ACRONYMS	iv
1.0 INTRODUCTION	1
2.0 CONCEPTUAL MODEL OF SUBSURFACE FLOW AND TRANSPORT.....	2
3.0 MODEL FORMULATION	3
3.1 Governing Equations	3
4.0 SITE-SPECIFIC EXAMPLE.....	5
4.1 Geology.....	7
4.2 Description of Nuclear Test.....	8
4.3 Boundary Conditions	9
4.4 Input Data.....	11
5.0 RESULTS OF SIMULATIONS	13
5.1 Porous Media Simulations	13
5.1.1 Heterogeneous Permeability Field.....	16
5.1.2 Temperature Gradients.....	27
5.1.3 Other Radionuclides.....	27
5.1.4 Fractures with 10-m Spacing.....	27
6.0 DISCUSSION.....	32
6.1 Observations Specific to Rio Blanco	32
6.2 General Observations Pertinent to all Sites	33
7.0 CONCLUSIONS.....	34
8.0 REFERENCES	34

LIST OF FIGURES

1. Permeability curves in semi-log space.....	6
2. Permeability curves in linear space.....	6
3. Boundary conditions for the simulations.....	10
4. Mass fraction of tritium in the gas phase (X_g^{3H}) for the homogeneous $k=3 \times 10^{-17} \text{ m}^2$ simulations at (a) 10 yrs, (b) 30 yrs, (c) 50 yrs, and (d) 100 yrs.....	14
5. Mass fraction of tritium in the liquid phase (X_l^{3H}) for the homogeneous $k=3 \times 10^{-17} \text{ m}^2$ porous media simulations at (a) 10 yrs, (b) 30 yrs, (c) 50 yrs, and (d) 100 yrs.....	17
6. Pressure field for homogeneous $k=3 \times 10^{-17} \text{ m}^2$ at (a) 10 yrs, and (b) 30 yrs.....	19
7. Mass fraction of tritium in the gas phase (X_g^{3H}) for homogeneous $k=3 \times 10^{-17} \text{ m}^2$ with no radioactive decay at 100 yrs.....	20
8. X_g^{3H} at (a) 50 years and (b) 100 years for homogeneous $k=3 \times 10^{-16} \text{ m}^2$	21
9. X_l^{3H} at (a) 50 years and (b) 100 years for homogeneous $k=3 \times 10^{-16} \text{ m}^2$	22
10. Permeability domain for heterogeneous simulations, with k varying as $1 \times 10^{-15} \text{ m}^2$ between 0 and 20 m from the cavity/chimney, $5 \times 10^{-15} \text{ m}^2$ from 20-40 m, $1 \times 10^{-16} \text{ m}^2$ from 40-60 m, $5 \times 10^{-16} \text{ m}^2$ from 60-80 m, and with $3 \times 10^{-17} \text{ m}^2$ for the rest of the computational domain.....	23
11. Mass fraction in tritium in the gas phase (X_g^{3H}) for (a) 10 yrs, (b) 30 yrs, (c) 50 yrs, and (d) 100 yrs for a heterogeneous permeability field.....	24
12. Mass fraction of tritium in the liquid phase (X_l^{3H}) for the same simulation as Figure 11..	26
13. Mass fraction of tritium in the gas phase (X_g^{3H}) for (a) 50 yrs, and (b) 100 yrs for the nonisothermal simulation.....	28
14. Fracture and matrix simulations at (a) and (b) 50 years and (c) and (d) 100 years for dual permeability simulations.....	29

LIST OF TABLES

1. Initial conditions for simulations.....	11
2. Values for tritium mass fraction of zero and one in each (gas and liquid) phase.....	12

LIST OF ACRONYMS

Ci	Curies
DOE	U.S. Department of Energy
pCi	picoCuries
TU	Tritium units

1.0 INTRODUCTION

The U.S. Atomic Energy Commission (predecessor to the U.S. Department of Energy, DOE) was responsible for nuclear weapons research and development as part of the national defense program during the 1960s and 1970s. In addition to underground testing of nuclear weapons, the commission oversaw a joint program between industry and government to develop technology for nuclear stimulation of low permeability gas reservoirs. Three experiments were fielded for this program: Project Gasbuggy in the San Juan Basin of northwestern New Mexico, and Projects Rulison and Rio Blanco in the Piceance Creek Basin of west-central Colorado.

The objective of the program was to produce natural gas from formations not conducive to production by conventional means (*e.g.*, hydraulic fracturing or acid fracturing). As a result, all of the tests were conducted in low permeability formations contained within oil and gas reservoirs. These conditions precluded contact of the test radionuclides with mobile, potable water, and hence the risk of human exposure was considered very low to non-existent. At the conclusion of each project in the late 1960s and early 1970s, surface facilities were removed, wells plugged and abandoned, and drilling restrictions instituted for the subsurface region immediately around the nuclear cavities.

In the 1990s, the DOE began a thorough environmental restoration program to remediate and close facilities that supported nuclear testing. The three gas-stimulation test sites are included in the program directed by the Nevada Operations Office, which is responsible for all underground nuclear testing. Though the land surfaces at the sites had previously been cleaned and closed, additional testing and analysis is being conducted to assure that the closures meet current environmental standards. Similarly, the disposition of the subsurface regions impacted by the tests will also be re-evaluated. Of particular concern for the subsurface is assessing if the drilling intrusion restrictions in place are sufficiently protective of human health and the environment. This concern arises from a lack of documentation on the rationale used to establish the restricted regions. Standard oil and gas reservoir evaluations are poorly suited to analyze the problem because they focus on flow of fluids in the subsurface, whereas the question here is one of transport of contaminants. Significant advances in understanding contaminant transport in the subsurface have been made in the decades since the drilling restrictions were established.

The purpose of this investigation is to develop a procedure for quantitatively analyzing the potential for radionuclide transport from the three gas-stimulation tests. This involves identifying the main transport processes that have occurred and are currently occurring in relation to the detonations, selecting analytical or numerical methods appropriate for calculating transport, and applying these methods to a test case using site-specific data. Subsequent studies will apply the approach to each site, estimate the extent of contamination in the reservoirs, and determine drilling exclusion zones protective of human health and the environment.

A conceptual model is developed to identify the key transport mechanisms; these ideas are implemented into a preliminary numerical model to test the significance of various phenomena affecting radionuclide transport rates. These results are also used to determine the sensitivity of the model to various parameters in identify key data to be collected either in the field or laboratory.

This report documents the modeling procedure, and discusses the results and sources of data for Rio Blanco as an example. Important parameters controlling the flow process are identified, as well as some bounds on flow and transport quantities. A key feature of the model is

that fractures are implemented discretely, rather than being incorporated as bulk features. That is, the more-common approach of including fractures as an effective continuum is replaced by a dual-permeability approach, where fractures are included discretely in the simulations.

2.0 CONCEPTUAL MODEL OF SUBSURFACE FLOW AND TRANSPORT

The geologic formations tested by the nuclear devices are characterized as low-permeability, two-phase, fractured gas reservoirs with a gas saturation (S_g) of ~ 0.6 . (Phase saturation is defined as the volume of a given phase divided by the volume of pores in a unit volume of rock.) Oil, if present, is disregarded as an active phase; however, there may be some oil present at the reservoir pressure and temperature. In a porous medium, the larger pores are typically filled with the nonwetting fluid (in this case, gas) while the smaller pores are filled with the wetting fluid (water). This follows from the Laplace equation, which states that within a pore of radius r , the phase pressure P and radius are inversely related as

$$P = \frac{\sigma \cos\theta}{2r} \quad (1)$$

Here, σ is the surface tension of the wetting fluid and θ is the contact angle through the wetting phase. If the porous medium is fractured, and the fracture aperture is typically larger than the characteristic pore diameter, the fractures will be filled with the gas phase fluid (Wang and Narasimhan, 1985). This is assumed to be the case: the permeability of the porous medium is so small that most gas production is through fractures. Both phases are assumed to be continuous throughout the reservoir; they flow in response to pressure gradients of each phase.

There are too many unknowns to include fractures realistically in the model. On one hand, the scale of the model is too small to include fractures discretely. On the other hand, fractures are too ordered and structured to include them stochastically. As a compromise, the fractures are modeled as a network of concentric squares where the fractures encompass the outer area, and the matrix encompasses the inner areas. This results in a tractable model of fractures in which the properties can be varied between simulations. This allows analysis of the quantitative effects of varying fracture properties.

In addition to the natural fractures in place, the nuclear detonations also create an extensive fracture zone, although the extent and degree of fracturing are unclear. These fractures extend generally radially around the devices. The Rio Blanco test consisted of three nuclear explosives at different depths in the borehole, so that vertical fracturing there may be enhanced.

Permeability enhancement of the rocks as a function of explosive charge is more poorly known than the extent of fractures created by the detonations. Although the detonations are believed to enhance fracture permeability, no data or models exist that describe either permeability enhancement or the fracture pattern as a function of explosive charge or distance from the detonation. Spatial variability of permeability was varied in the simulations to investigate the relationship. With respect to porosity, fractures created from the detonations probably did little to enhance it, as fractures usually contribute little to porosity.

One effect of the detonations was the release of a large number of neutrons that ionized the pore water and resulted in high tritium concentrations in the subsurface. Since tritium is an isotope of hydrogen, it is able to form radioactive water molecules. These molecules exist in both the liquid and gas phase, and are capable of being exchanged between phases. Detonation of the devices created a concentration gradient of tritium; in addition to the pressure-driven flow,

radionuclides are transported in both phases by diffusion and dispersion in the porous medium and fractures. The fracture permeability is higher than the permeability of the porous medium such that the most rapid transport mechanism is flow of tritiated gas through fractures. However, two retardation mechanisms exist that may significantly reduce the distance and rate of transport. The most significant is that diffusion of tritium gas from the fractures to the matrix (matrix diffusion) will reduce the concentration of tritium in the fractures. The second is that tritium is radioactive with a half-life of 12.26 years; its daughter product is nonradioactive hydrogen. The degree to which these retardation mechanisms affect transport will be clear when the interplay among the flow rate through fractures, matrix diffusion of tritium gas, and radioactive decay are understood.

3.0 MODEL FORMULATION

The TOUGH2 (Pruess, 1987; Pruess *et al.*, 1999) integral finite difference computer program was chosen to implement the model as it handles multiphase, multicomponent heat and mass transport for a dual continuum (fractures plus matrix) in a fully coupled manner. Local thermodynamic equilibrium is assumed such that phase pressures, temperatures, densities, and viscosities in either fractures or porous media are the same within any REV (representative elementary volume) at any time. The equation of state module that was implemented contains five components: water, air, heat, a radionuclide with first-order decay, and its daughter product. The TOUGH2 simulator has been successfully tested against analytical solutions of heat and mass transport such as two-dimensional infiltration with gravity, diffusion and dispersion of solutes in groundwater, geothermal fluid production and injection, and transport of volatile organic vapors in an unsaturated zone (Pruess, 1987; Pruess *et al.*, 1999). Enhancements include phase partitioning based upon Henry's law and vapor pressure lowering as a function of temperature and concentration of dissolved solutes.

3.1 Governing Equations

The two fluid phases are gas (water vapor and air) and liquid water. As little is known of the thermodynamic properties of the gas mixtures at the three nuclear-stimulation sites, the gas phase was left as air instead of replacing it with methane properties. The governing mass and heat transport equations are

$$\frac{d}{dt} \int_{V_n} M^\kappa dV_n = \int_{\Gamma_n} \mathbf{F}^\kappa \cdot \mathbf{n} d\Gamma_n + \int_{V_n} q^\kappa dV_n \quad (2)$$

where the integration is over the domain of the flow system, V_n , which is bounded by the closed surface Γ_n . The quantity M that appears in the accumulation term represents mass or energy per unit volume, where the components (mass and/or heat) are labeled by κ ($\kappa=1$ water, $\kappa=2$ air, $\kappa=3$ heat). \mathbf{F} denotes mass or heat flux, and q denotes sources and sinks. The normal vector \mathbf{n} on the surface $d\Gamma_n$ points inward into V_n .

The mass accumulation term is

$$M^\kappa = \phi \sum_{\beta} S_{\beta} \rho_{\beta} X_{\beta}^{\kappa} \quad (3)$$

The total mass of component κ is obtained by summing over the fluid phases β (liquid, gas). ϕ is porosity, S_β is saturation of phase β , ρ_β is the density of phase β , and X_β^κ is the mass fraction of component κ in phase β . The heat accumulation term is

$$M^3 = (1-\phi)\rho_r C_r T + \phi \sum_{\beta} S_\beta \rho_\beta u_\beta \quad (4)$$

where ρ_r is the grain density of the porous medium, C_r is the specific heat of the rock, T is temperature, and u_β is the internal energy of phase β .

Mass flux terms are summed over the two mobile phases,

$$\mathbf{F}^\kappa = \sum_{\beta} X_\beta^\kappa \mathbf{F}_\beta^\kappa \quad (5)$$

and the flux of each phase is modeled by the multiphase version of Darcy's law

$$\mathbf{F}_\beta = \rho_\beta \mathbf{u}_\beta = -k \frac{k_{r\beta} \rho_\beta}{\mu_\beta} (\nabla P_\beta + \rho_\beta \mathbf{g}) \quad (6)$$

Here, \mathbf{u}_β is the Darcy velocity of phase β , k is absolute permeability, $k_{r\beta}$ is the relative permeability to phase β , μ_β is the dynamic viscosity of phase β , and ∇P_β is the pressure gradient across phase β .

Heat flux (conduction and convection) is

$$\mathbf{F}^3 = -\lambda \nabla T + \sum_{\beta} h_\beta \mathbf{F}_\beta \quad (7)$$

where λ is thermal conductivity, and h_β is the specific enthalpy of phase β .

Mass diffusion for both solutes and gases is modeled with Fick's law,

$$\mathbf{f}_\beta^\kappa = -\phi \tau_\phi \tau_\beta \rho_\beta D_\beta^\kappa \nabla X_\beta^\kappa \quad (8)$$

where \mathbf{f}_β^κ is the mass flux of component κ in phase β , ϕ is porosity, τ_ϕ is a tortuosity parameter dependent upon pore geometry, τ_β is a tortuosity parameter dependent upon phase saturation, D_β^κ is the diffusion coefficient of component κ in phase β , and X_β^κ is the mass fraction of component κ in phase β . The hydrodynamic dispersion module available in TOUGH2 was not implemented in these simulations; there are no data on dispersivities, and since properties of the fractures themselves are largely unknown, dispersion would only contribute to uncertainty. Fortunately, the primary interest is in radionuclide transport in the gas phase, and unlike the case for liquids, mass flux due to gas diffusion in porous media and fractures is more important than gas dispersion. A scale analysis shows why: the diffusion coefficient, D , for gases is $\sim 10^{-5} \text{ m}^2 \text{ s}^{-1}$. For gas flow through porous media, a maximum velocity might be 10^{-4} m s^{-1} (about 10 m day^{-1}), and a dispersivity value (a characteristic pore diameter) for a medium-grained sandstone (used in the site example presented below) might be 10^{-6} m . The hydrodynamic dispersion coefficient, D_h ,

would be $D_h = \alpha u \sim 10^{-10} \text{ m}^2 \text{ s}^{-1}$, which is five orders of magnitude smaller than the molecular diffusion coefficient for a typical gas. Gas dispersion is usually only of concern for very high velocity flow around boreholes.

The capillary pressure function is unknown in the formations at these sites; neither are models known for capillary pressure in fractures, as little is known about the physics of two-phase flow in fractures. Rather than use an untested model without knowledge of the parameters, an assumption is made that there is no capillary pressure between the two phases, *i.e.*, $P_{cap} = P_g - P_l = 0$. The significance is that flow is due primarily to viscous and gravity forces. Similarly, nothing is known about the proper model of relative permeability, therefore, a simple model was developed for consolidated media in which the relative permeability is a function of liquid saturation (Corey, 1954; 1994):

$$\begin{aligned} k_{rl} &= \hat{S}^4 \\ k_{rg} &= (1 - \hat{S})^2 (1 - \hat{S}^2) \\ \hat{S} &= \frac{S_l - S_{lr}}{1 - S_{lr} - S_{gr}} \end{aligned} \quad (9)$$

Here, k_{rl} is the relative permeability to the liquid phase, k_{rg} is the relative permeability to the gas phase, S_{lr} is the residual saturation of the liquid phase, and S_{gr} is the residual saturation of the gas phase. Figure 1 shows the permeability to liquid (k_l) and gas (k_g) in semi-log space, as a function of liquid saturation. The curves do not sum to unity, indicating that the model allows for interference between the two phases as a function of the viscosity ratio between the two fluids (Bear, 1988). Figure 2 shows the permeabilities as a function of saturation, in linear space.

Fractures created from the detonations are incorporated physically in the model. That is, instead of parameterizing fracture matrix interaction with an effective term, they are modeled explicitly as multiple interacting continua (Pruess and Narasimhan, 1985), which extends the dual continuum model of Warren and Root (1963). Although there are estimates of the extent of fracturing as a function of distance from the cavities, there are no good models that predict fracture density as a function of distance from the cavities.

4.0 SITE-SPECIFIC EXAMPLE

The conceptual and numerical approach described above is tested by a preliminary application to one of the gas-stimulation tests. Project Rio Blanco was the third experiment under the gas-stimulation program; it was the first experiment in the United States where three nuclear explosives were detonated simultaneously in the same emplacement well. The three 33-kiloton nuclear explosives were placed in a 2,134-m well (RB-E-01) at 1,780, 1,899, and 2,039 m below the land surface and detonated on May 17, 1973 (U.S. Department of Energy, 2000). Although the formations were extensively fractured, subsequent drilling and testing indicated that the permeability between the location of the upper and lower nuclear devices had actually decreased, rather than increased. Of several reasons given for this, the most plausible is that the initial estimates of permeability were exaggerated (Toman, 1975). At least one additional well was

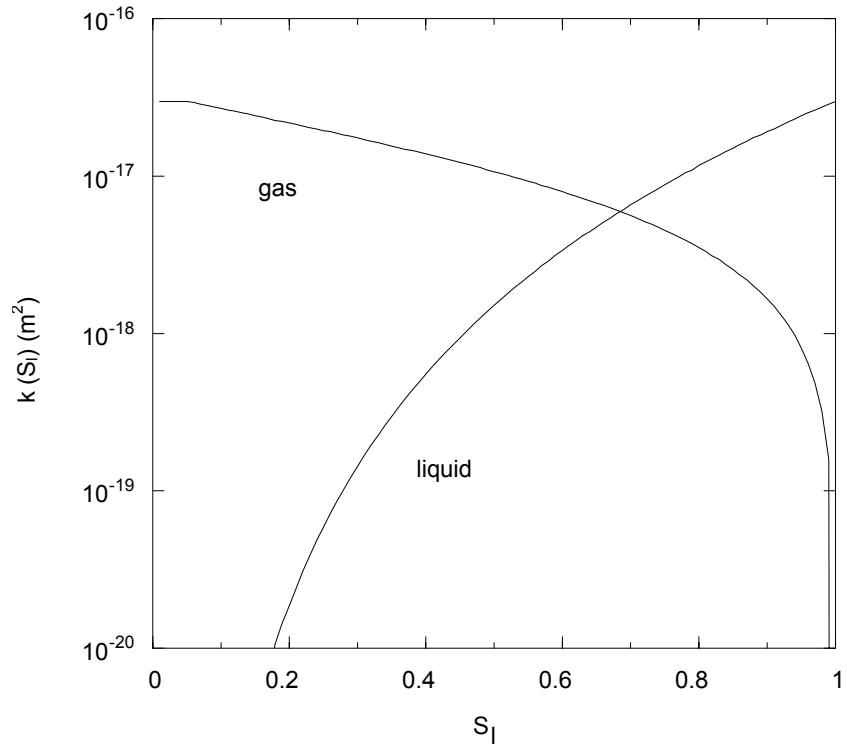


Figure 1. Permeability curves in semi-log space.

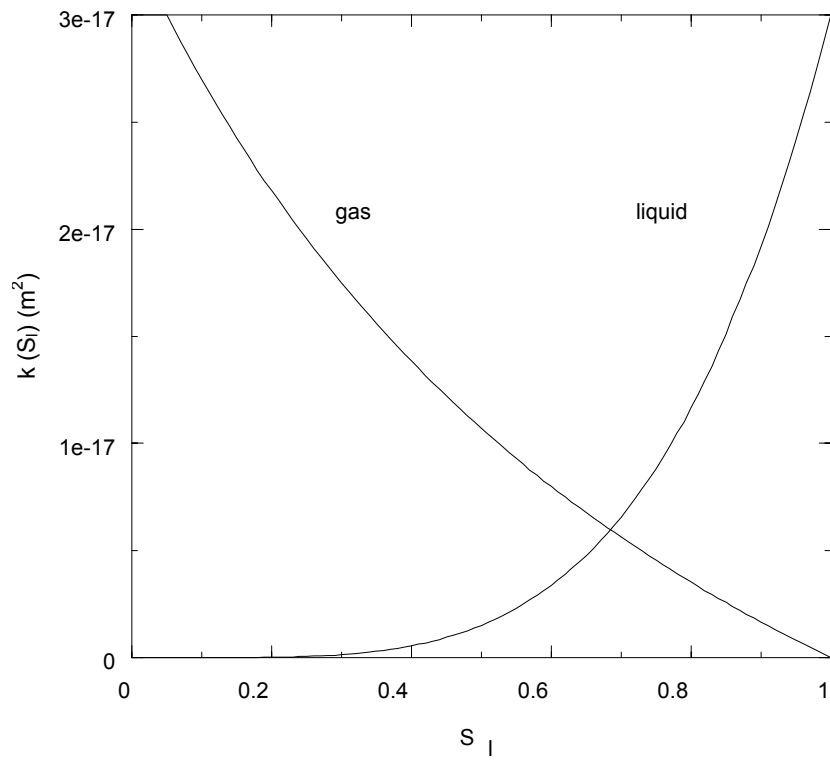


Figure 2. Permeability curves in linear space.

planned to penetrate the region between the middle and lower devices; however, it is not clear if it or any other wells were ever drilled. Hence, little is known of the effects of the detonations on fracture permeability between the middle and lower devices.

The Upper Cretaceous Mesaverde Formation or Group (its status is not well defined) forms a low-permeability, two-phase, fractured gas reservoir with a gas saturation (S_g) ~ 0.6 . The pre-test permeability was estimated to range from 10^{-15} m² to nearly 8×10^{-18} m² (CER Geonuclear, no date); however, this is probably the permeability of the fractures and not the matrix. Although the post-test drilling indicated no fracture connectivity between the upper and lower devices, an assumption is made that the connectivity is based upon the scale analysis reported by Toman and Tewes (1972).

Fracturing from the three explosives is assumed to be cylindrical. An assumption that vertical fracture connectivity scales with distance is made and is in accordance with the relationship reported by Toman and Tewes (1972). This assumption is conservative; that is, it results in an overestimate in permeability. With respect to fracturing in the horizontal direction, Toman (1975) estimates that fractures probably extend to 60 m. The pre-test sandstone porosity is estimated as 10.5 percent (CER Geonuclear, date unknown).

4.1 Geology

All three nuclear devices were detonated in the Upper Cretaceous Mesaverde Formation or Group in the Piceance Creek Basin of Western Colorado (Hansley and Johnson, 1980). The upper device was detonated in the Ohio Creek Member of the Mesaverde; it was originally reported to have been detonated in the Paleocene Fort Union Formation (CER Geonuclear, no date), but the stratigraphy was revised based upon pollen analyses (Hansley and Johnson, 1980).

The Piceance Creek Basin is a structural and sedimentary basin formed during the Laramide orogeny, from latest Cretaceous through Paleocene time (Johnson, 1989). Deposition of the Upper Cretaceous Mesaverde Formation or Group in the basin mostly predates the Laramide orogeny. The dip of the Mesaverde is not strictly known in the vicinity of the emplacement well. However, the structure of the underlying Jurassic Dakota Sandstone is known, and is to the northeast at 0.0861 m/m (Rocky Mountain Map Co., 1999). Because the Mesaverde and Dakota sandstones underwent the same orogeny, and therefore have similar tectonic history and deformation, it is assumed that both formations have the same strike and dip.

The thickness of the Ohio Creek Member is not known exactly. The Fort Union formation was originally reported as 245 m thick (CER Geonuclear, no date). Core collected from the vicinity of the upper two nuclear devices was described as medium- to coarse-grained feldspathic sandstone (potassium and sodium feldspar, quartz) with irregular and contorted laminae (presumably from deposition of finer grains) and with chert and quartzite pebbles scattered throughout the interval (Hansley and Johnson, 1980). Lower in the formation, near the location of the lower device, the petrography is similar although the grains are somewhat finer. Minor detrital components include biotite, chlorite, and muscovite. Permeability of the Mesaverde Formation is very low due primarily to the intense diagenesis that filled pores with quartz, authigenic feldspar, dolomite, calcite, and illite (Pitman *et al.*, 1989). Diagenesis probably began before the sediments were deeply buried.

The Mesaverde Formation is regionally fractured as a result of regional tectonism (Pitman and Sprunt, 1986). Several mechanisms were responsible for fracturing: anisotropic

horizontal compression, elevated pore pressure, and deep burial of sediments (Lorenz *et al.*, 1991). High formation pressure was essential to creating low effective stresses and brittle rock properties at depth, but was probably not the direct cause of fracturing. Quartz and calcite crystal overgrowths have been observed in the Mesaverde, indicating that fractures can be open below surface (Lorenz *et al.*, 1991). Although there have been studies related to development and mechanics of fractures, there have been no published studies on their hydraulic properties.

The Mesaverde is informally divided into two parts. These are a lower marine part with blanket gas reservoirs and an upper nonmarine (primarily fluvial) part with mostly discontinuous lenticular reservoirs. Most of the gas produced has been from the marine section, although the fluvial section probably contains more gas (Johnson, 1989). This gas, however, is harder to produce due to the small size (tens to hundreds of meters in width) of the lenticular reservoirs. Johnson (1989) suggests that most, if not all gas production in the Mesaverde Formation or Group is from fractures. Although fractures are common in the Mesaverde (Lorenz and Finley, 1991), little is known of their distribution, connectivity, and hydraulic properties.

The gas reservoirs are unconventional as they cut across stratigraphic units, are commonly structurally downdip from water-saturated formations, and have no obvious trapping mechanism (Johnson, 1989). Most of the gas is probably thermally generated and is derived from organically rich portions of the Mesaverde and underlying Mancos Shale. Gas formation began during the Eocene and ended approximately 10 m.y. ago, at which time gas generation ceased as formation temperatures lowered due to down-cutting of the Colorado River system (Johnson, 1989). In general, the low-permeability gas reservoirs do not have discrete gas/water contacts in any of the fields within the Piceance Basin. Accurate measurements of pressure are largely absent, as most drill-stem tests were not run to completion because the pressure buildup time was very slow due to the extremely low permeability (Ronald Johnson, U.S. Geological Survey, personal communication, 2000). The Mesaverde Formation is overpressured throughout much of the Piceance Creek Basin; in the study area it is presumed normally pressured (Johnson, personal communication). Below 3,000 m in the study area, the formation is thought to be overpressured. Much of this evidence is derived from mud weights used during drilling (Johnson, 1989), although the absence of radionuclide contamination in the overlying aquifers weakly suggests that the Mesaverde Formation may be normally pressured.

4.2 Description of Nuclear Test

The discussions on mechanical effects such as rock fracturing, cavity formation, and pressure history associated with the detonation are from Toman and Tewes (1972), Taylor (1972), Beaver (1972), and Toman (1975). They are partly derived from models of detonations in other formations that have been scaled to the formation properties at Rio Blanco.

Production tests in a nearby well (Fawn Creek Government No. 1) indicated that the formation pressure prior to detonation was 19.2 MPa (CER Geonuclear, no date). The three 33-kiloton nuclear explosives were simultaneously detonated at 1,780, 1,899, and 2,039 m below the land surface. Within 10 seconds of the blast, the formation pressure exceeded the lithostatic pressure, causing extensive fracturing of the Mesaverde and Fort Union formations (Toman and Tewes, 1972). The extreme temperatures from the blast vaporized much of the rock, water, and gas, resulting in an underground cylindrical cavity with a volume on the order of $1.3 \times 10^5 \text{ m}^3$ ($\sim 10^9$ kg of rock). Within one minute of the detonation, the formation pressure fell to pre-detonation formation pressure (19.2 MPa). Molten rock formed a puddle of lava several meters

deep at the bottom of the cavity. It is not known if a chimney formed in the cavity; typically when the gas pressure can no longer sustain the weight of the roof of the cavity in an underground nuclear explosion, the roof collapses into the cavity, which forms a chimney. There is no surface expression suggesting the formation of a chimney, nor did post-drilling confirm or deny the formation of a chimney.

Within several days, the cavity/chimney cooled to below 600 K, and condensation of steam began. At this time, the rate of cooling of the cavity/chimney gas sharply decreased. Within one month, most of the steam condensed, causing formation pressure to drop to 11.1 MPa; at this point the condensed steam flowed into the chimney, which resulted in a rise back to pre-test formation pressure in the cavity/chimney.

The detonation created extensive fracturing in the Mesaverde Formation. The three cavity radii (R_c) were each estimated as 21 m. A scale analysis by Toman and Tewes (1972) suggests that for explosives spaced closer than $7 R_c$, fractures have a “high probability” of being connected between test points. At Rio Blanco, the upper and lower explosives were both spaced within $7 R_c$ of the middle explosive; hence, it was highly probable that vertical fracture connectivity existed between all three explosives. The degree of fracturing, however, is unknown. With reference to conditions at the Nevada Test Site, Borg *et al.* (1976) states that from the cavity out to $1.3 R_c$, the rocks are “highly” crushed. From $2.5-4R_c$, the rocks are “pervasively” crushed. Beyond 3.5 to $4 R_c$, there are probably no fractures.

Although the detonation enhanced fracture permeability, no data or models exist that describe permeability enhancement as a function of distance from the detonation. Based upon a questionable relationship between permeability and porosity/specific surface, McKee and Hanson (1975) showed that permeability decreases with radius from the detonation as r^{-5} for spherical blasts and r^{-4} around a cylindrical blast. No data or models exist that relate explosive yield to fracture orientation or fracture density.

Although the model predicted hydraulic connection between the three cavities, post-test drilling indicated that no connection existed between the middle and upper cavities (Toman, 1975). A hole drilled to within either 36 m or 76 m (both numbers are reported in the report) of the point of the uppermost device was completed six months after the detonation. Two production tests revealed that there was no communication between the uppermost chimney and the lower ones, as there was no significant amount of tracer incorporated in the center explosive canister detected in the produced gas. Although plans were made to drill into the middle and lower chimneys, there appear to be no published reports on these activities.

Tritium radioactivity released from the three simultaneous detonations was 3,000 Ci (curies). Forty percent of this radioactivity was trapped in the melt. The initial partitioning of the remaining radioactivity between phases is discussed in the input data section.

4.3 Boundary Conditions

The boundary conditions are prescribed pressure and radionuclide concentration at the cavity radius. An infinite, vertical half plane is simulated; that is, the outer boundary is prescribed pre-detonation formation pressure, and zero concentration of radionuclides. The upper and lower boundaries are more difficult to define: it is assumed that the underlying Mancos shale is an impermeable unit to flow and transport, and the upper boundary is infinite. Simulations show that radionuclides are confined to within a few hundred meters above the location of the

top device. The simulations are of two-dimensional, vertical cross sections; there are not enough data to warrant three-dimensional simulations.

The computational domain is a two-dimensional, Cartesian, vertical cross section 800 m tall (z -direction) by 1,000 m long (x -direction) evenly discretized into 20 m x 20 m grid blocks. Figure 3 shows the domain with the boundary conditions. The left-hand boundary is the edge of the cavity, that is, one R_c from the initial borehole. The boundary conditions here are prescribed pressure, solute concentration, and (for nonisothermal simulations) geothermal temperature gradient. The right-hand boundary conditions (away from the cavity) are prescribed (constant) pressure, zero concentration, and zero temperature (again, for nonisothermal simulations). The upper boundary condition is prescribed pressure, zero concentration of solute and constant temperature (for nonisothermal simulations). The lower boundary condition is no flow of fluids or flux of mass or heat.

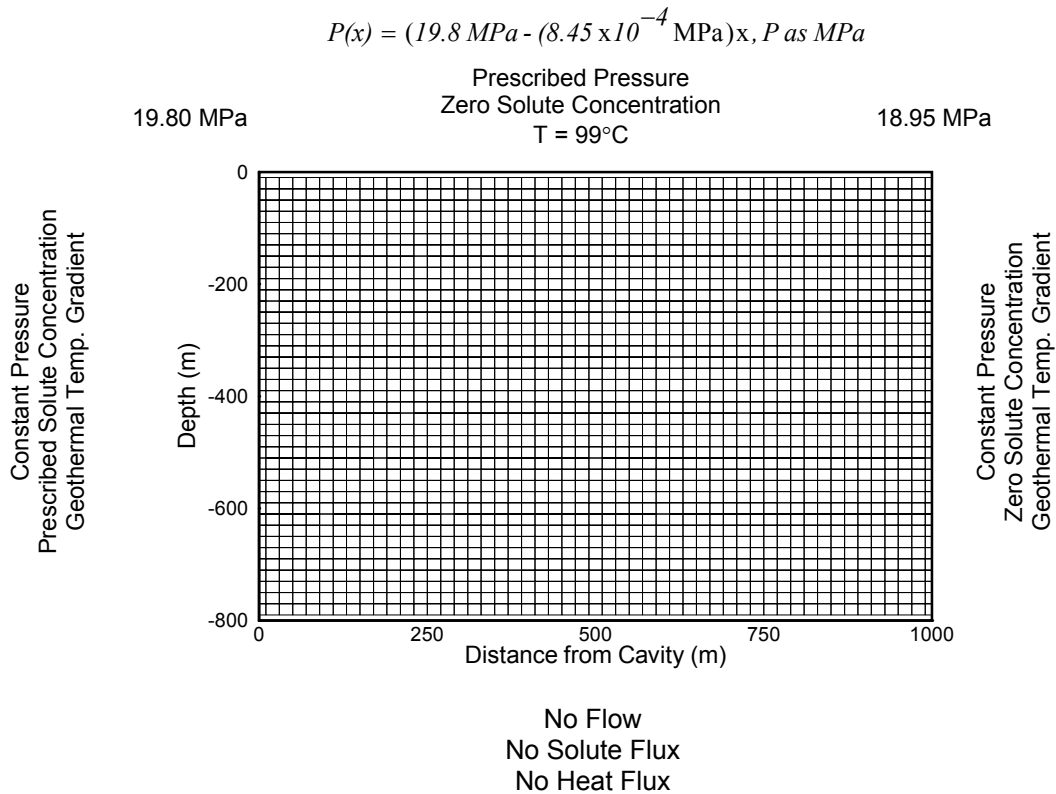


Figure 3. Boundary conditions for the simulations.

Simulations were run for 120 years (approximately 10 half-lives of tritium). By this time, most of the mass had decayed to the stable daughter (He, in the case of tritium) such that the maximum extent of tritium contamination had been reached.

4.4 Input Data

Table 1. Initial conditions for simulations.

Parameter	Value	Source
Intrinsic permeability, m ²	3 x 10 ⁻¹⁷	CER Geonuclear reservoir report
Relative permeability	K _r =S ^d	Corey, 1954
Capillary pressure	None	
Porosity	0.105	CER Geonuclear reservoir report
Pressure, Pa	1.895 x 10 ⁷	CER Geonuclear reservoir report
Formation dip, m m ⁻¹	0.0861	Structure contour map, Rocky Mtn Map Co., 1999
Liquid saturation	0.4	CER Geonuclear reservoir report
Gas saturation	0.6	CER Geonuclear reservoir report
Tritium radioactivity, curies	1800	Toman and Tewes, 1972
Mass fraction tritium in liquid	7.2 x 10 ⁻¹²	calculated from Toman, 1972
Diffusion coefficient, tritium in air, m ² s ⁻¹	8.87 x 10 ⁻⁵	Reid et al., 1987
Diffusion coefficient, tritium in liquid water, m ² s ⁻¹	3.47 x 10 ⁻⁹	Mills, 1973
Diffusion coefficient, helium air, m ² s ⁻¹	6.58 x 10 ⁻⁵	Cussler, 1997
Diffusion coefficient, helium in liquid water, m ² s ⁻¹	6.28 x 10 ⁻⁹	Cussler, 1997
Diffusion coefficient, methane in liquid water, m ² s ⁻¹	1.49 x 10 ⁻⁹	Cussler, 1997
Tritium half-life, yr	12.26	Faure, 1977

Diffusion coefficients measured at 25° C
 Formation assumed hydrostatically pressured, therefore pressure gradient computed from structural control

The amount and types of radionuclides released from the three detonations are known only theoretically. Of the radionuclides posing a threat to the accessible environment, tritium and krypton are of most concern as these occur in large concentration in the gas phase, and are therefore the most mobile. Radioactivity from tritium was estimated as 3,000 Ci (Toman and Tewes, 1972). Of this, 40 percent was trapped in the melt and is considered immobile over the timescale of concern in this assessment (*i.e.*, ~100 years). During production testing, 28 Ci were injected into the Mesaverde through an injection well (Fawn Creek Government No. 1; injection depth 1,716 to 1,851 m below surface) located in the same section as the emplacement hole, 22.9 Ci were flared as dry gas, and 0.1 Ci was flared as water vapor (U.S. Energy Research and Development Administration and Continental Oil Company, 1975). The remaining 1,749 Ci were dissolved in 2.6 x 10⁷ kg liquid water (Toman and Tewes, 1972). TOUGH2 requires input of radionuclide concentration as mass fraction. The conversion from radioactivity of tritium (Ci) to mass fraction in the liquid phase (X_l^{3H}) is as follows:

$$\begin{aligned}
 & \left(\frac{1749 \text{ Ci}}{2.6 \times 10^{10} \text{ gr } H_2O} \right) \left(\frac{TU}{3.2 \text{ pCi/l } H_2O} \right) \left(\frac{10^{12} \text{ pCi}}{\text{Ci}} \right) \left(\frac{10^3 \text{ gr } H_2O}{\text{l } H_2O} \right) \left(\frac{10^{-18} \frac{\text{atoms } ^3H}{\text{atom } H}}{TU} \right) \\
 & \left(\frac{\text{mol } ^3H \text{ atoms}}{6.03 \times 10^{23} \text{ atoms } ^3H} \right) \left(\frac{3 \text{ g } ^3H}{\text{mol } ^3H} \right) \left(\frac{6.03 \times 10^{23} \text{ atoms } H}{\text{mol } H} \right) \left(\frac{\text{mol } H}{1 \text{ gr } H} \right) \left(\frac{2 \text{ gr } H}{18 \text{ gr } H_2O} \right) \\
 & = 7.0 \times 10^{-12} \frac{\text{gr } ^3H}{\text{gr } H_2O}
 \end{aligned}$$

TU is the abbreviation for Tritium Units, while pCi is the abbreviation for picocuries (one picocurie is 10^{-12} Curies).

TOUGH2 requires all radionuclides to be entered as mass fraction in the liquid phase; as such, all of the radioactivity (1,749 Ci) was assumed to be in the liquid water. Although this is not strictly a correct assumption, the radionuclides partition themselves within the first few time steps based upon Henry's law. Mass fraction is the mass of radionuclides per total mass of components in the system, and is a dimensionless value scaled between zero and one. Table 2 shows the values for "zero" (background concentrations in nature) and "one" for tritium in each phase. (For the liquid phase, "zero" is defined as 1 pCi per liter H₂O).

Table 2. Values for tritium mass fraction of zero and one in each (gas and liquid) phase.

	Gas phase	Liquid phase
$X^{3H} = 0$	1.70×10^{-15}	1.04×10^{-19}
$X^{3H} = 1$	6.80×10^{-8}	7.00×10^{-12}

Reliable formation pressure data are difficult to obtain for the Mesaverde because the shut-in pressure buildups are much too low to be extrapolated to the formation pressures (Johnson, 1989). No data were found on the initial formation pressure in the emplacement well RB-E-01; however, the initial formation pressure was measured as 19.2 MPa (CER Geonuclear, no date) in the Fawn Creek Government No. 1 well. This value is consistent with a hydrostatically pressured reservoir. There is some information on the change in formation pressure during the production tests that were conducted subsequent to the detonations. Upon re-entry into the cavity and/or chimney six months after the detonations, the initial bottom hole formation pressure was measured as 14.1 MPa at either 1,704 m or 1,744 m below land surface (again, both depths were reported in Toman, 1975). The first drawdown test produced 10^6 m³ of gas, while the bottom hole pressure dropped to 8.7 MPa. A 69-day shut-in period followed, during which time the bottom hole pressure rose to 11.6 MPa. A second drawdown test was then begun, lasted 19 days, and produced 1.776×10^6 m³ of dry gas. The final shut-in pressure at the end of the test was 3.1 MPa. Beyond this time, there are no data on the pressure buildup in the well. Although there are data on pressure transients during the various production tests, no data with respect to the spatial distribution of pressure are known during those tests. As a result, the pre-detonation Fawn Creek Government No. 1 formation pressure of 19.2 MPa was used as the boundary condition pressure at the chimney/cavity. In lieu of these data, a hydrostatic representative of the depth was calculated as 19.80 MPa, which was used as the formation pressure.

With respect to the formation pressure gradient, it was assumed that the pressure gradient is structurally controlled. That is, that the patterns of flow and transport are confined to the Mesaverde and Fort Union formations so that the formation depth defines the formation pressure gradient. A structure contour map (Rocky Mountain Map Co., 1999) was used to determine the formation dip; in the vicinity of the emplacement well, the Dakota Sandstone (the formation for which the structure is accurately known) dips to the northeast at 0.086 m m^{-1} . At 1,000 m away, the pressure is 18.95 MPa.

Although the Mesaverde is probably highly heterogeneous, there is no information on the degree of heterogeneity, or the spatial scale over which heterogeneity may correlate. Because of

the lack of data on heterogeneity, the formation is modeled as homogeneous and isotropic. To account for this oversimplification, several simulations were conducted to investigate the effect of a higher permeability on radionuclide transport. The values of permeability probably reflect the permeability of the natural fractures; the reason follows from statements that actual gas production is from fractures, rather than from the matrix.

The diffusion coefficients for tritium and krypton-85 in binary gases at low pressures were estimated from empirical correlations based upon Chapman and Enskog (as reported in Reid *et al.*, 1987, eq. 11-3.2). However, diffusion occurs in the formation at an elevated pressure on the order of 19 MPa. The effect of pressure on diffusivity using the correlation developed by Takahashi (1974; see also Reid *et al.*, 1987, eq. 11-5.1) was investigated. For the reservoir conditions at Rio Blanco, the diffusion coefficients changed only by 2 percent, well within the uncertainty of the estimates at low pressure. Therefore, the pressure-adjusted diffusion coefficients were not used for either component.

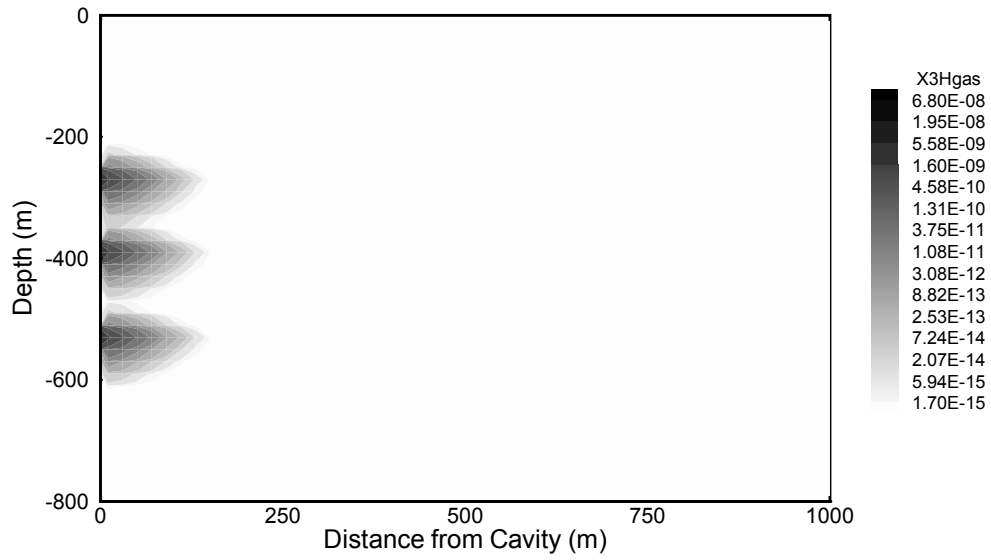
5.0 RESULTS OF SIMULATIONS

The results are shown somewhat heuristically; that is, to start, basic simulations for a porous medium (no fractures) are used to understand the particulars of the flow and concentration fields. Most of the processes and associated effects can be understood in terms of the porous media simulations. Permeability heterogeneity is introduced next, and then both horizontal and vertical temperature gradients are added. Finally, a simulation is run to show the effects of fractures.

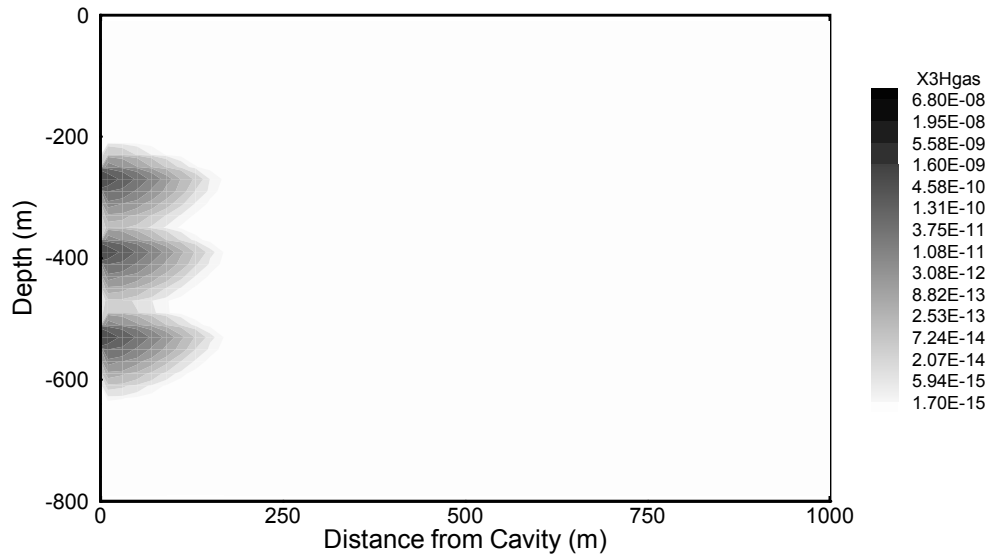
The basic input data for all simulations are shown in Table 1. However, some variables were changed to investigate their effect; for example, one simulation discussed below has a spatially variable permeability field. Deviations from the input data in Table 1 are discussed as they pertain to specific simulations.

5.1 Porous Media Simulations

Mass fraction of tritium in the gas phase (X_g^{3H}) at different times is shown in Figure 4a-d. Here, the homogeneous and isotropic permeability is $3 \times 10^{-17} \text{ m}^2$. Detonation of the three nuclear devices results in development of three separate tritium plumes. In all figures, the left-hand boundary is actually the outer edge of the cavity/chimney, and not the location of the detonations themselves. The edge of the cavity/chimney was estimated to be 20 m from the location of each device. As discussed above, the reason for not including the cavity/chimney in the model is that there is little understanding of the mechanics of mixing within the cavity/chimney. Within the first 10 years, tritium from the detonations in the gas phase has reached approximately 175 meters. There has been essentially no vertical mixing of tritium among the three sources. At 20 years, the shape of the plume is similar, although it has extended to approximately 200 m past the boundary. By 50 years (a little more than four half-lives), tritium has extended out to approximately 200 m. The horizontal extent of the plume is essentially at steady state, as the growth of the plume is balanced by the decay of tritium. By 100 years, the shape of the plume is similar to that at 40 years, although the maximum tritium concentration (at the source) is nearly two orders-of-magnitude less than the original concentration. Finer discretization would show more refinement but would not show any new features.

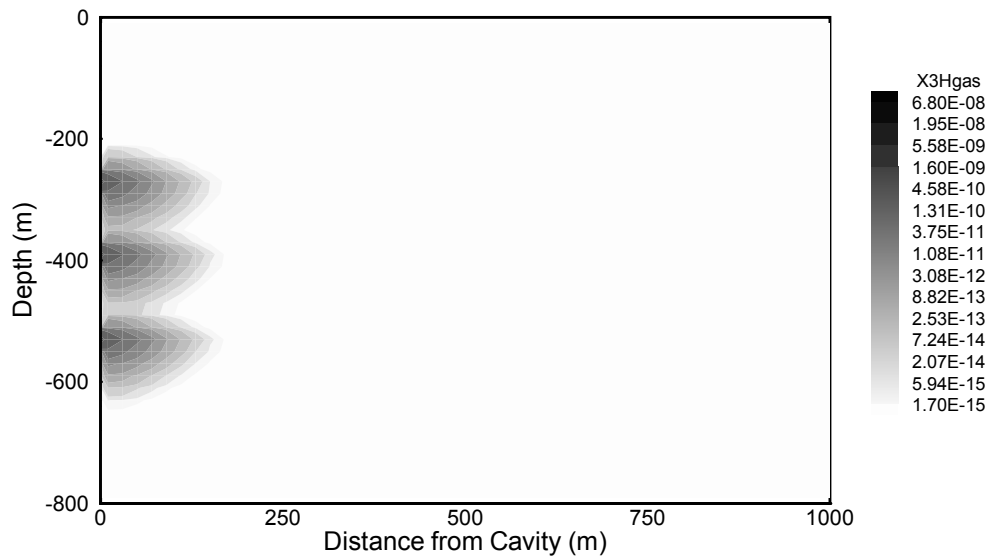


(a)

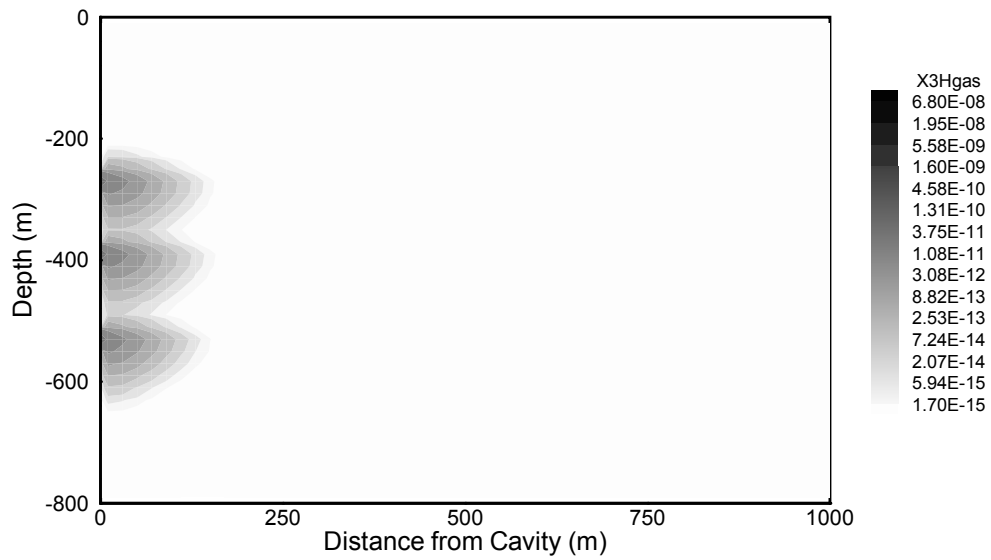


(b)

Figure 4. Mass fraction of tritium in the gas phase (X_g^{3H}) for the homogeneous $k=3 \times 10^{-17} \text{ m}^2$ simulations at (a) 10 yrs, (b) 30 yrs, (c) 50 yrs, and (d) 100 yrs.



(c)



(d)

Figure 4. Mass fraction of tritium in the gas phase (X_g^{3H}) for the homogeneous $k=3 \times 10^{-17} \text{ m}^2$ simulations at (a) 10 yrs, (b) 30 yrs, (c) 50 yrs, and (d) 100 yrs (continued).

Tritium mass fraction in the liquid phase (X_l^{3H}) for the same times as above is shown in Figure 5a-d. The shape of the plume for X_l^{3H} is similar to tritium mass fraction in the gas phase, although the X_l^{3H} plume appears slightly more diffuse. There is slightly more vertical mixing of tritium in the liquid phase between the three plumes, and the extent of tritium contamination is slightly further than for the gas phase (it extends to approximately 250 m). However, the actual concentrations in the liquid phase are less than for the gas phase, as the mass fractions are normalizations to different values. That is, the total amount of tritium available in the gas phase is greater than for the liquid phase, due to Henry's law considerations.

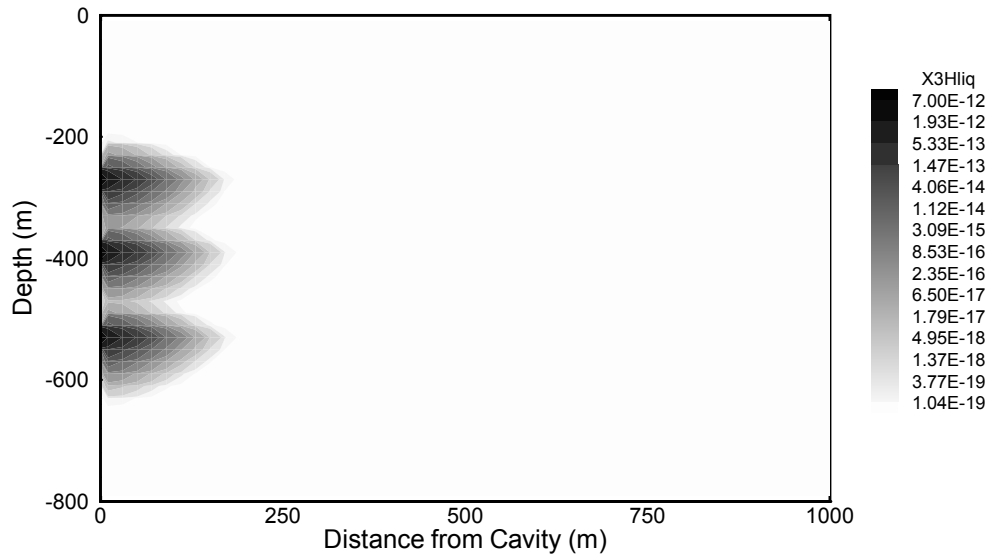
The pressure field at 10 yrs and 20 yrs is shown in Figure 6. In the left-hand side of the domain, the field is dominated by the regional horizontal pressure gradient. The importance of gravity is seen toward the right-hand side of the domain. Analysis of the pressure field at later times shows that it has essentially stabilized by 20 years, that is, that it has nearly reached a condition of steady state.

The effect of decay of tritium is seen in Figure 7, which shows X_g^{3H} at 100 years. Tritium contamination extends to approximately 260 m from the cavity/chimney, and X_g^{3H} at the original source location is the same as the initial condition.

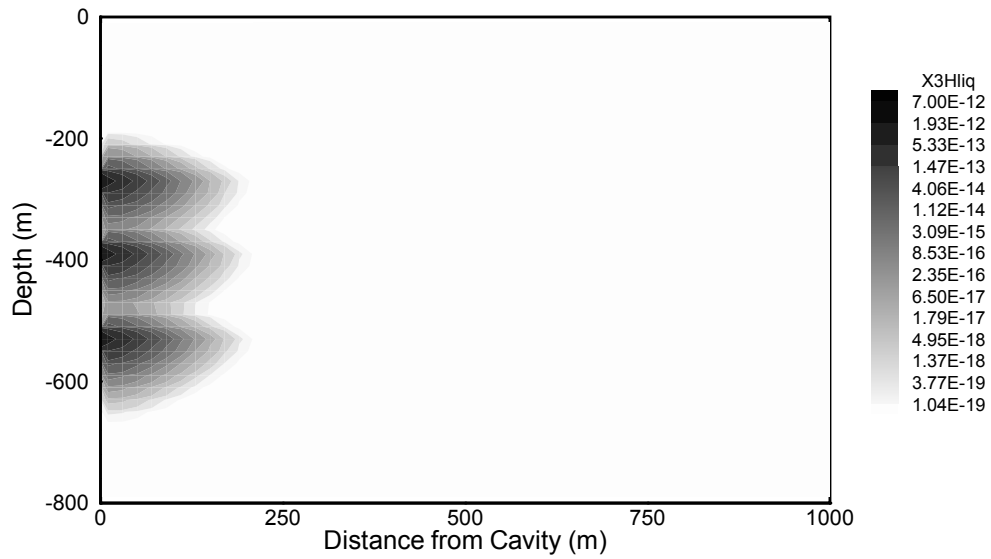
Although the $3 \times 10^{-17} \text{ m}^2$ value used for permeability is thought to be an overestimate (Toman, 1975; however, a more realistic value was never suggested), a one order-of-magnitude increase in k essentially doubles the extent of tritium in the horizontal direction. Figures 8 and 9 show X_g^{3H} and X_l^{3H} at 50 and 100 years for $k = 3 \times 10^{-16} \text{ m}^2$. The extent of tritium contamination is contained within 500 m of the edge of the cavity/chimney. Within the first 10 years, the three plumes have mixed because of the high permeability; by 30 years, the plume has reached 250 m and is influenced by the bottom boundary. Ideally, the domain would be made larger so that the boundary would not be "felt"; however, the dimensions were chosen so that all of the figures could be compared without having to change scale. By 50-years simulation time, the plume has reached a nearly steady state: any further progress is dampened by the consequent decay of tritium.

5.1.1 Heterogeneous Permeability Field

As a first step in estimating the effects of fractures on flow and transport, a heterogeneous permeability field was simulated with intrinsic k variations as $1 \times 10^{-15} \text{ m}^2$ between 0 and 20 m from the cavity/chimney, $5 \times 10^{-15} \text{ m}^2$ from 20-40 m, $1 \times 10^{-16} \text{ m}^2$ from 40-60 m, $5 \times 10^{-16} \text{ m}^2$ from 60-80 m, and with $3 \times 10^{-17} \text{ m}^2$ for the rest of the computational domain (Figure 10). The results are shown in Figures 11 and 12. Figure 11 shows that the higher permeability in the near field (*i.e.*, within 80 m of the cavity/chimney) results in more rapid transport and higher gas phase tritium concentration in this area when compared to the homogeneous simulations for $k=3 \times 10^{-17} \text{ m}^2$. There is much more vertical mixing between the sources due to the much higher intrinsic permeability in their region. Tritium transport extends to approximately 225 m; most of this distance is reached within the first 10 years. Past this time, horizontal transport has reached nearly steady state except for tritium decay. The higher permeability results in downward drainage of liquid, carrying solutes within it. Drainage of liquid reaches the lower permeability layer, and essentially stops. This drainage is the result of gravitational and viscous forces (there

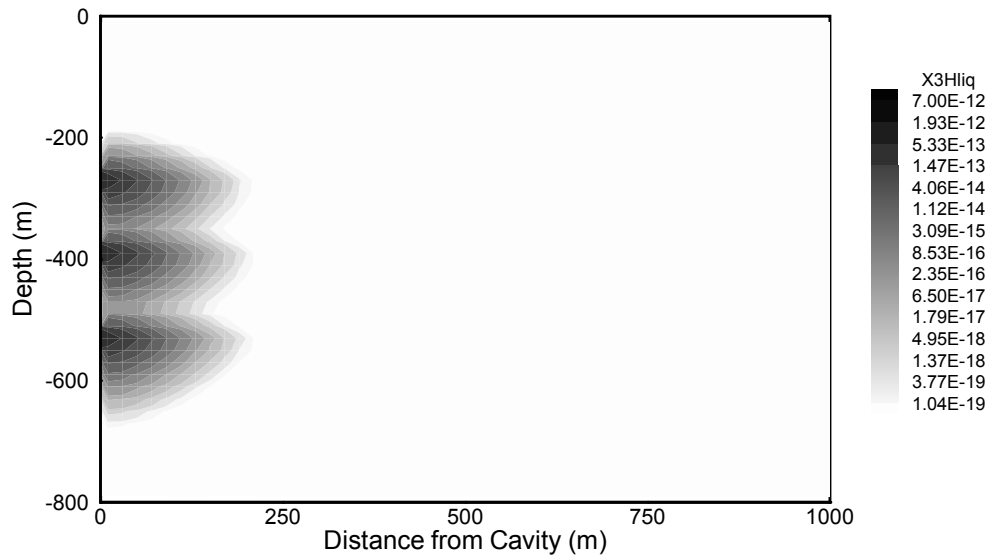


(a)

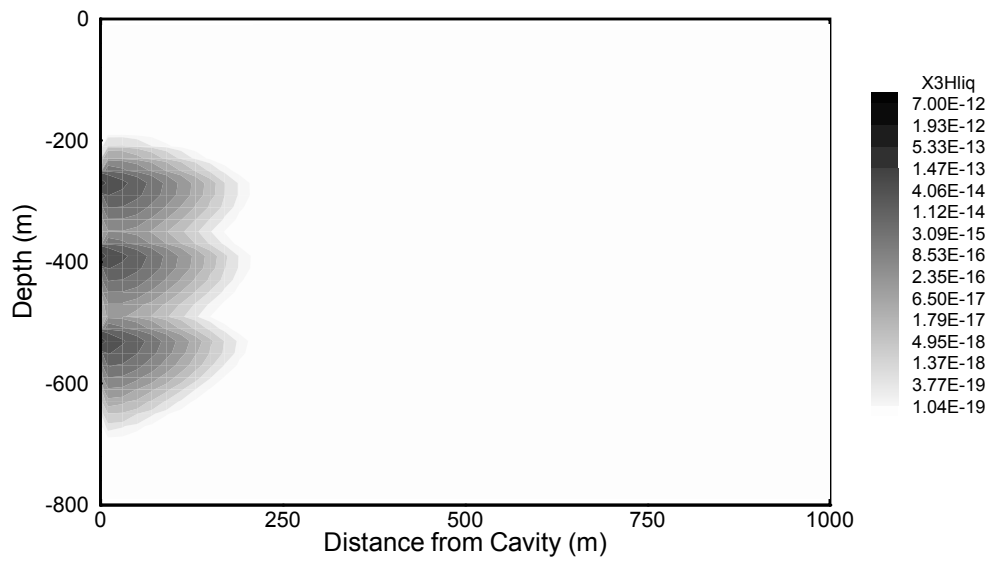


(b)

Figure 5. Mass fraction of tritium in the liquid phase (X_l^{3H}) for the homogeneous $k=3 \times 10^{-17} \text{ m}^2$ porous media simulations at (a) 10 yrs, (b) 30 yrs, (c) 50 yrs, and (d) 100 yrs.

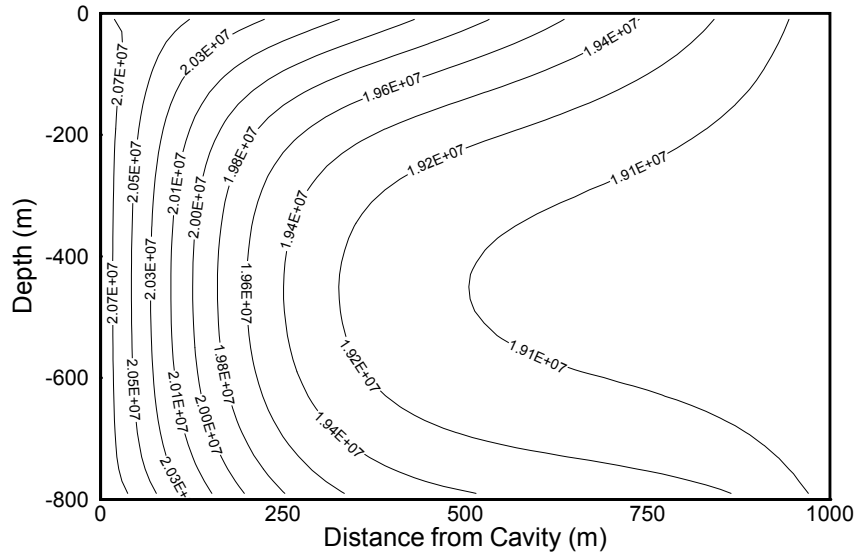


(c)

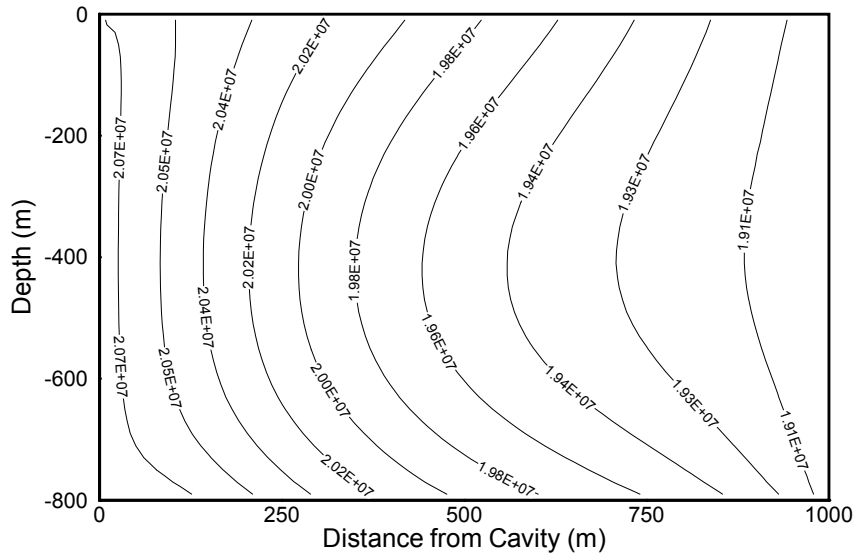


(d)

Figure 5. Mass fraction of tritium in the liquid phase (X_l^{3H}) for the homogeneous $k=3 \times 10^{-17} \text{ m}^2$ porous media simulations at (a) 10 yrs, (b) 30 yrs, (c) 50 yrs, and (d) 100 yrs (continued).



(a)



(b)

Figure 6. Pressure field for homogeneous $k=3 \times 10^{-17} \text{ m}^2$ at (a) 10 yrs, and (b) 30 yrs. The pressure field has nearly reached a condition of steady state by 30 yrs.

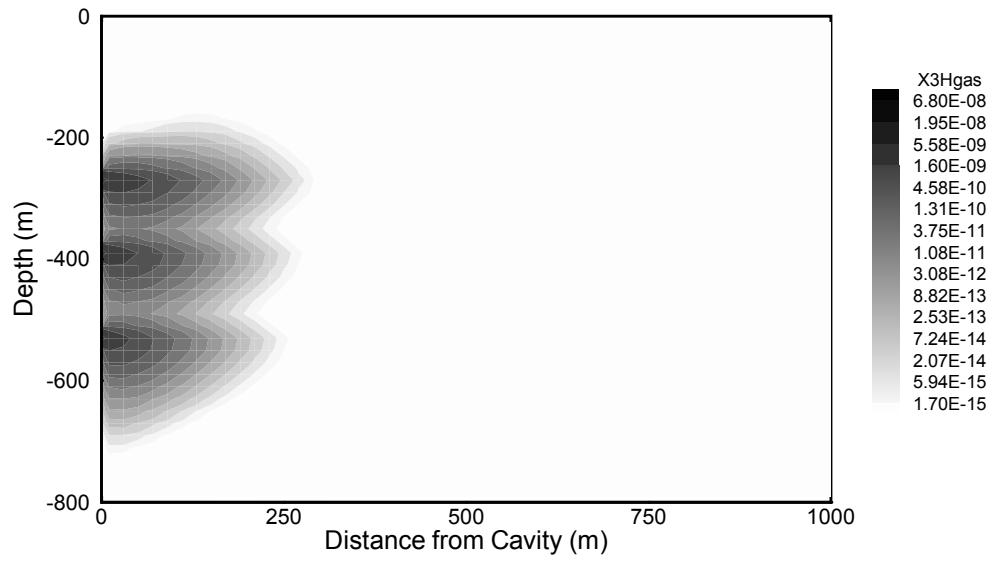
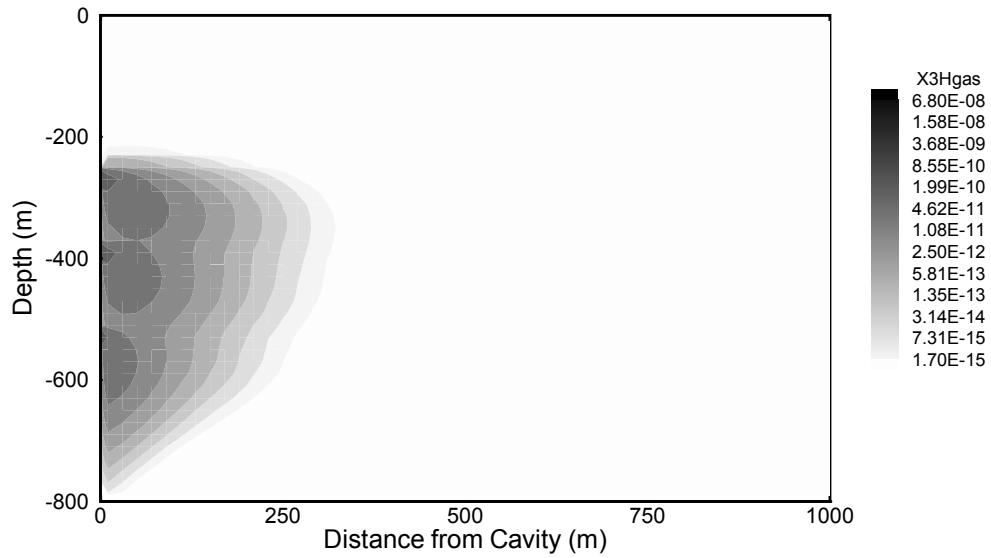
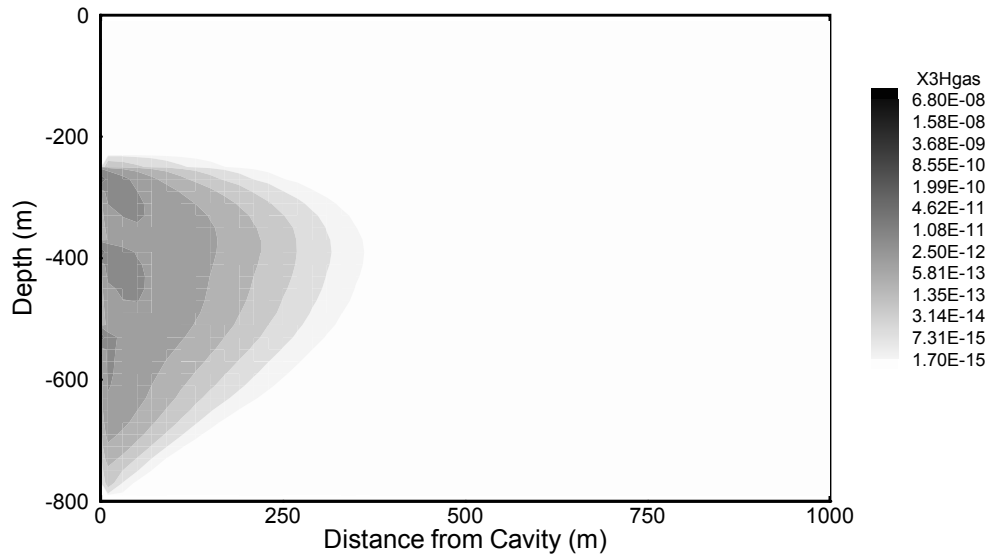


Figure 7. Mass fraction of tritium in the gas phase (X_g^{3H}) for homogeneous $k=3 \times 10^{-17} \text{ m}^2$ with no radioactive decay at 100 yrs.

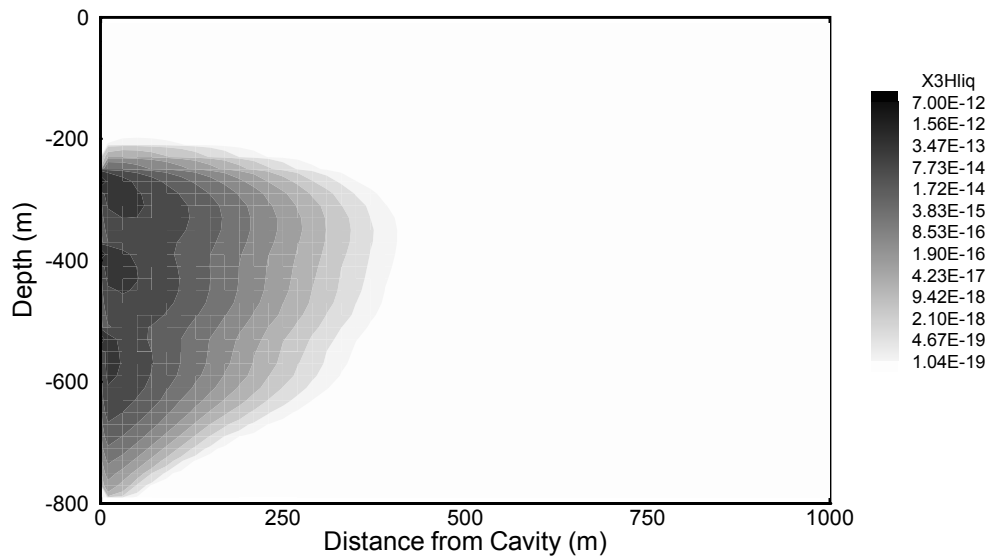


(a)

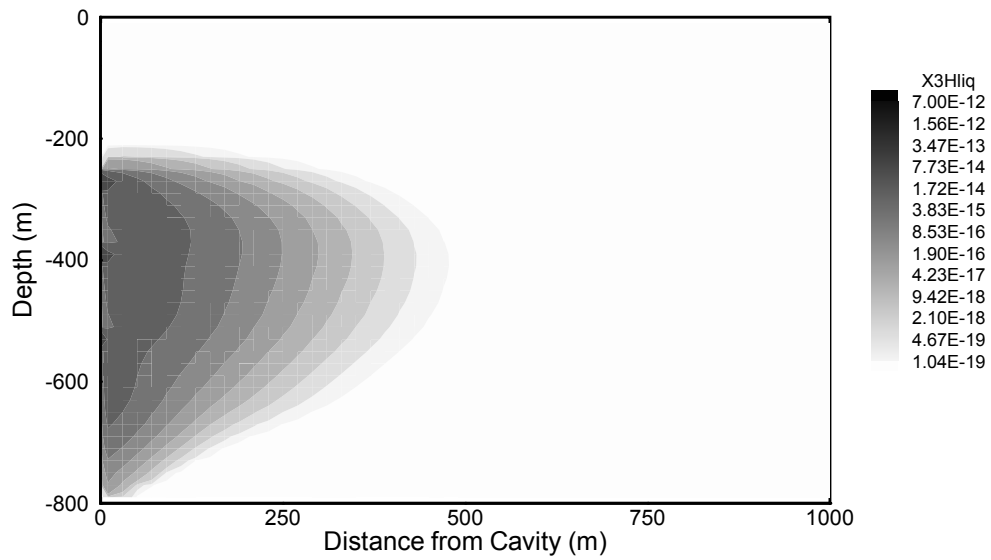


(b)

Figure 8. X_g^{3H} at (a) 50 years and (b) 100 years for homogeneous $k=3 \times 10^{-16} \text{ m}^2$. The absence of vertical transport within 100 m of the left-hand boundary is because the pressure contours in this region are nearly vertical, resulting in mostly horizontal flow. In addition, the grid spacing is too coarse to properly resolve tritium diffusion in this region.



(a)



(b)

Figure 9. X_l^{3H} at (a) 50 years and (b) 100 years for homogeneous $k=3 \times 10^{-16} \text{ m}^2$. See text and Figure 8 for the reason for the near absence of upward transport within 100 m of the left-hand boundary.

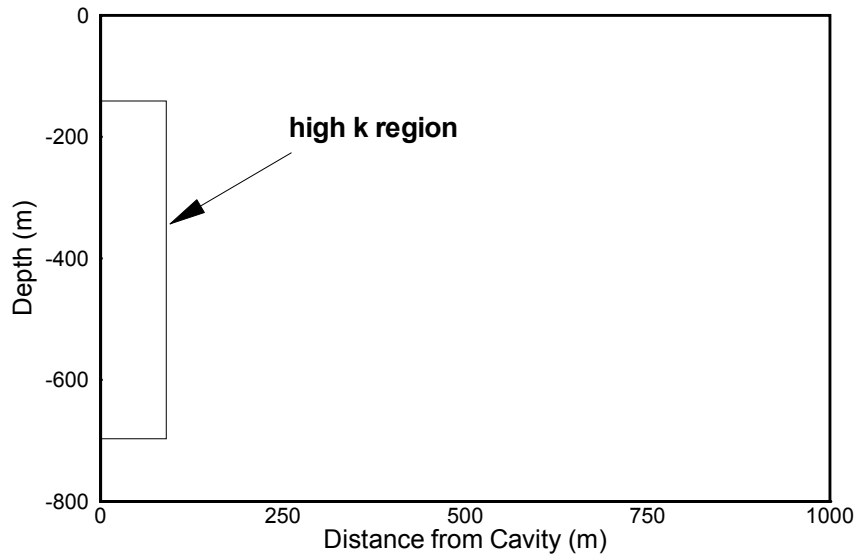
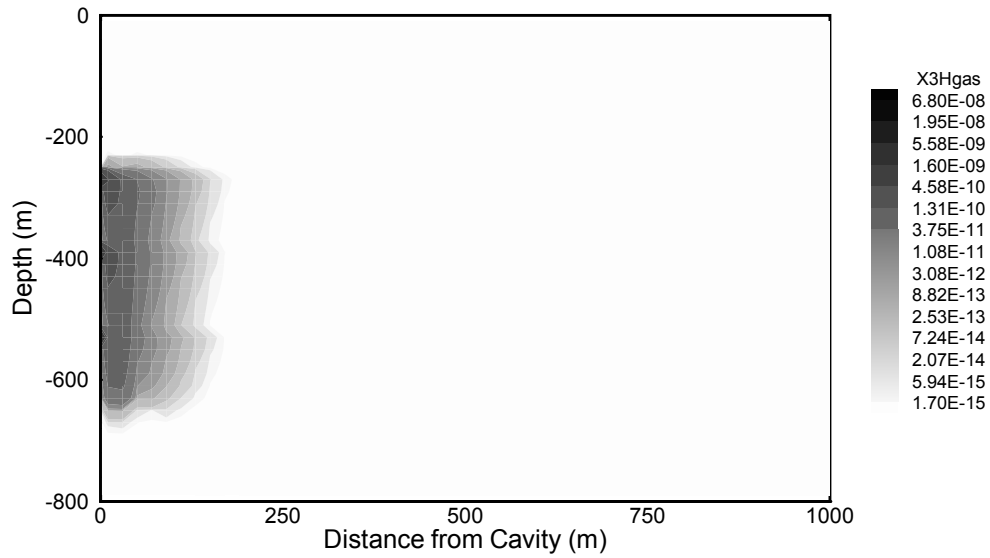
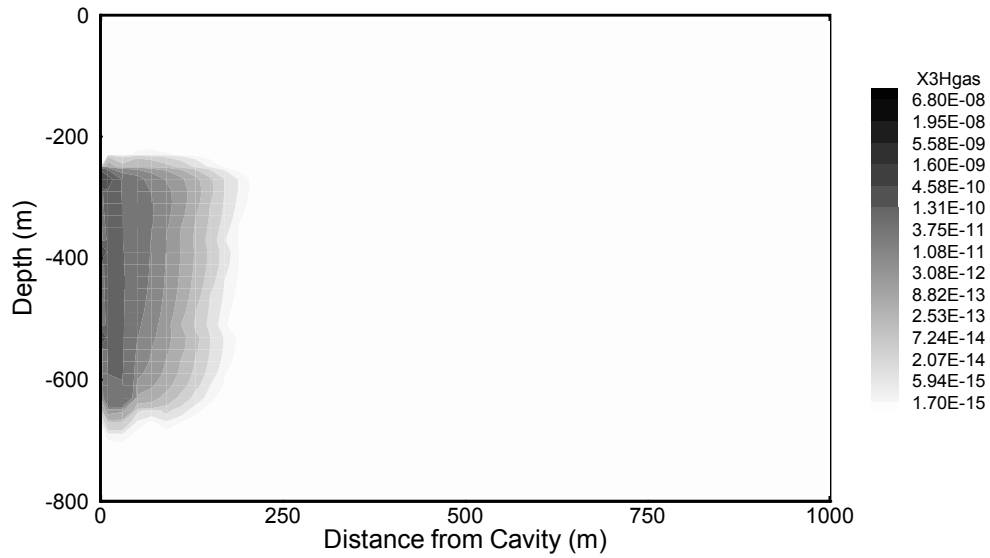


Figure 10. Permeability domain for heterogeneous simulations, with k varying as $1 \times 10^{-15} \text{ m}^2$ between 0 and 20 m from the cavity/chimney, $5 \times 10^{-15} \text{ m}^2$ from 20-40 m, $1 \times 10^{-16} \text{ m}^2$ from 40-60 m, $5 \times 10^{-16} \text{ m}^2$ from 60-80 m, and with $3 \times 10^{-17} \text{ m}^2$ for the rest of the computational domain. The upper and lower boundaries of the permeability field extend to $5R_c$ (100 m) from the upper and lower test points.

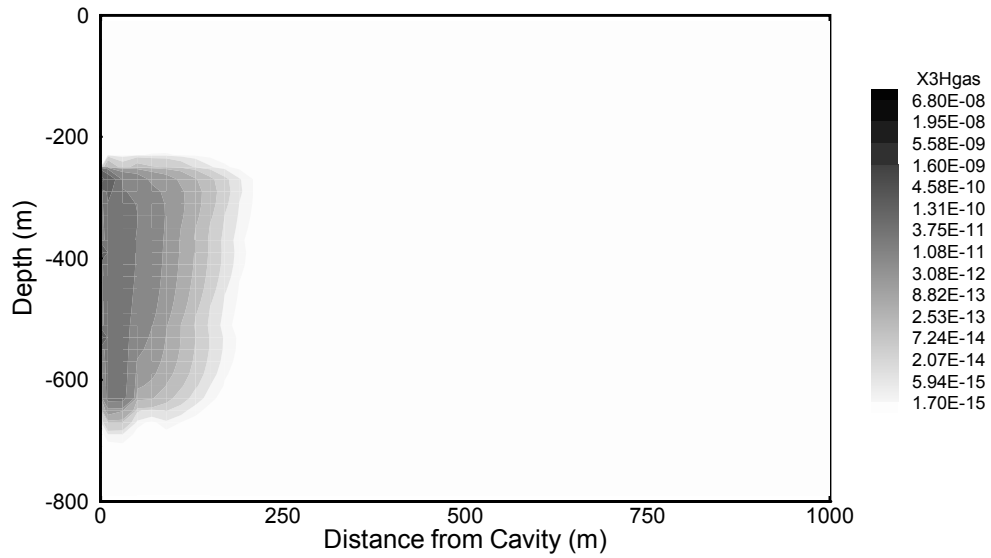


(a)



(b)

Figure 11. Mass fraction in tritium in the gas phase (X_g^{3H}) for (a) 10 yrs, (b) 30 yrs, (c) 50 yrs, and (d) 100 yrs for a heterogeneous permeability field. The intrinsic permeability field ranges from 10^{-15} m^2 to $5 \times 10^{-16} \text{ m}^2$ between the cavity/chimney edge and 80 m. Intrinsic permeability in the rest of the domain is $3 \times 10^{-17} \text{ m}^2$.

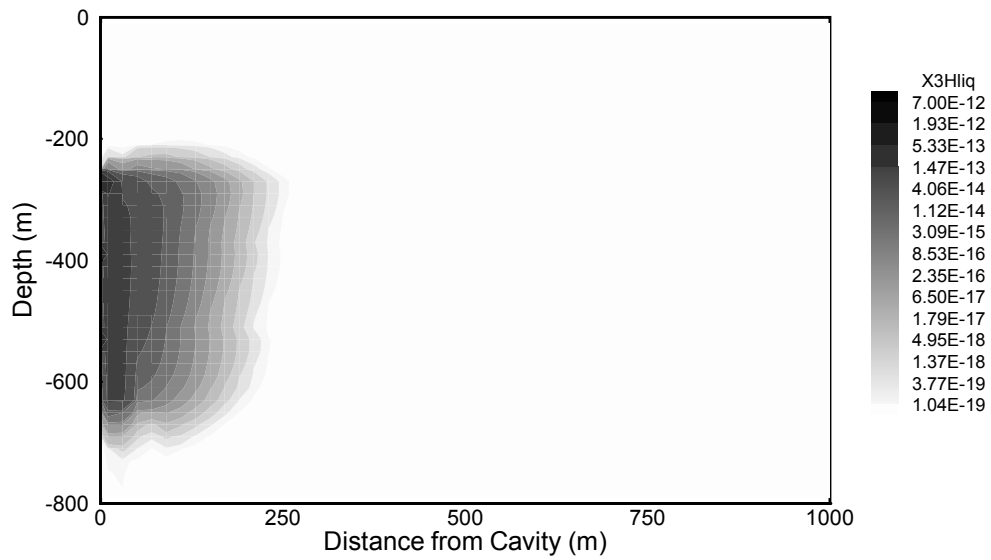


(c)

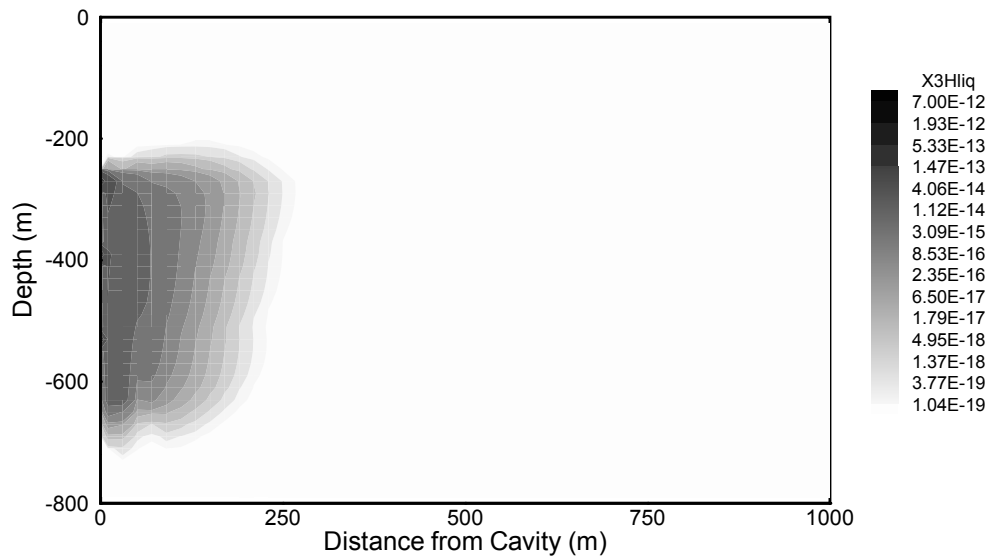


(d)

Figure 11. Mass fraction in tritium in the gas phase (X_g^{3H}) for (a) 10 yrs, (b) 30 yrs, (c) 50 yrs, and (d) 100 yrs for a heterogeneous permeability field. The intrinsic permeability field ranges from 10^{-15} m^2 to $5 \times 10^{-16} \text{ m}^2$ between the cavity/chimney edge and 80 m. Intrinsic permeability in the rest of the domain is $3 \times 10^{-17} \text{ m}^2$ (continued).



(a)



(b)

Figure 12. Mass fraction of tritium in the liquid phase (X_{3H}) for the same simulation as Figure 11. The times are (a) 50 yrs, and (b) 100 yrs.

is no capillarity). The reason that high tritium concentration exists in the gas phase is that as the liquid drains downward, it exchanges tritium with the gas phase, resulting in high tritium concentrations in that phase. There may also be downward transport of tritium in the gas phase due to its higher molecular weight than the decay product ($3 \text{ gr mol}^{-1} \text{ } ^3\text{H}$ vs. $1 \text{ gr mol}^{-1} \text{ He}$); however, this effect is minor in relation to the more predominant phase exchange process. Figure 12 shows mass fraction of tritium in the liquid phase at 50 and 100 years; its extent is slightly further (to nearly 250 m) from the cavity/chimney than tritium in the gas phase.

5.1.2 Temperature Gradients

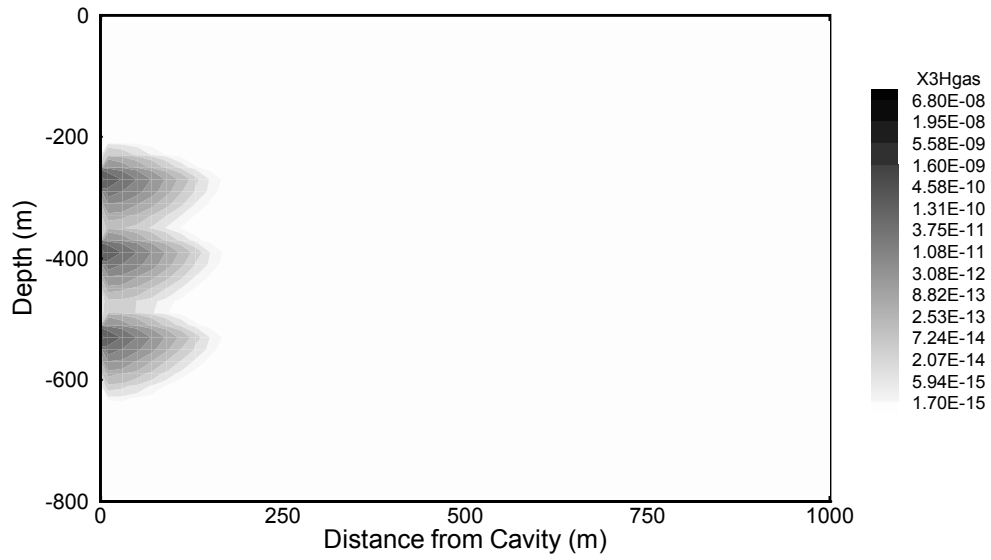
Temperature can have an important effect on transport through changes in the flow field due to buoyancy. Several simulations were run to investigate the role that temperature might have on the transport of tritium. A temperature field was imposed by incorporating a “typical” geothermal gradient of 1°C per 40 m. The upper boundary was held constant at 99°C , while the lower boundary was held constant at 119.5°C . The temperature gradient was imposed on the left and right boundaries -- 0.5°C per grid block (the grid blocks are 20 m x 20 m). In addition, a residual temperature perturbation was assumed from the detonations at the three sources. Almost no information exists on the temperature field after a detonation: a 50°C increase at the location of the sources was assumed, which may have been likely within several years of the detonation. Temperature effects are normally subtle in environments not prone to high thermal gradients or heat flux. The effects of a temperature field would be most noticeable in the homogeneous k simulations ($k = 3 \times 10^{-17} \text{ m}^2$) where the transport field is most uniform (*i.e.*, the simulations pertaining to Figures 4 and 5). The results are shown in Figure 13 for 50 and 100 years after the detonations. X_g^{3H} is nearly indistinguishable from the isothermal simulations with the same parameters (Figure 4 c,d). The elevated temperature at the three sources is not enough to induce effects to change the tritium concentration field.

5.1.3 Other Radionuclides

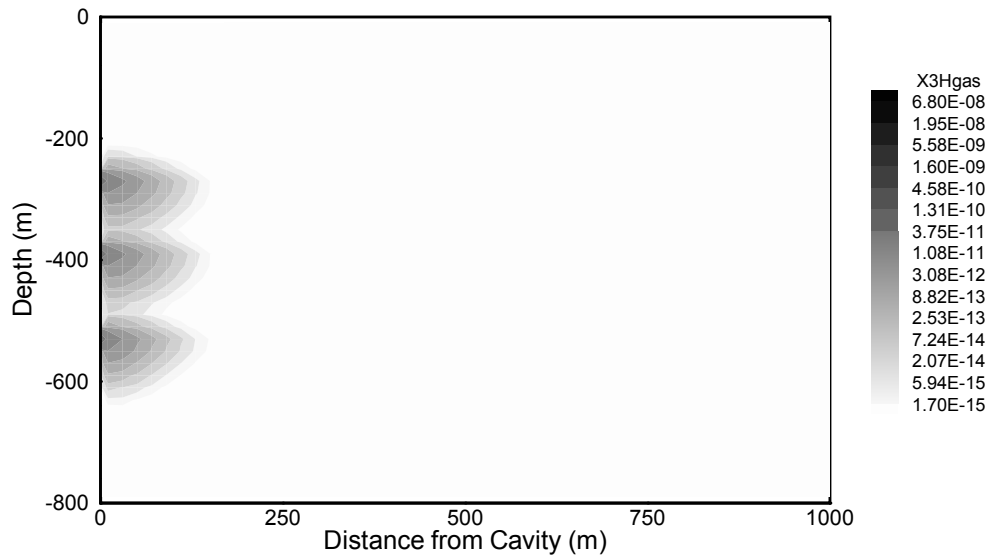
The initial tritium radioactivity was 3,000 Ci and was the most predominant radionuclide in the cavity gas. The only other radionuclide of importance to transport is krypton-85, which had an initial radioactivity of 2,000 Ci. All other species were present at much lower activities. Diffusion coefficients of krypton could not be found in either air or methane; however, the calculated diffusion coefficient is approximately 20 percent less than the value for tritium. The krypton diffusive flux is therefore always less than that of tritium, in accordance with Equation (8); that is, the diffusive flux of krypton is less than the diffusive flux of tritium because both the krypton concentration gradient and the diffusion coefficient are smaller. This was tested in a simulation using krypton properties, and confirmed. Therefore, the tritium concentration profiles reflect the worst-case scenario for radionuclide transport.

5.1.4 Fractures with 10-m Spacing

Figure 14 presents results of a simulation incorporating discrete fractures. Two sets of orthogonal fractures were generated with 10-m spacing and incorporated from the cavity/chimney boundary to a distance of 80 m. The intrinsic permeability of both the fractures and matrix in this simulation was 10^{-17} m^2 . Figure 14 a,b shows tritium mass fraction in the gas phase in fractures and matrix throughout the simulation domain. Figure 14 c,d shows flow only through the matrix. Although the matrix and fracture permeability are the same in this simulation, a different flow evolves for both matrix and fractures because the fracture porosity



(a)



(b)

Figure 13. Mass fraction of tritium in the gas phase (X_{g}^{3H}) for (a) 50 yrs, and (b) 100 yrs for the nonisothermal simulation.

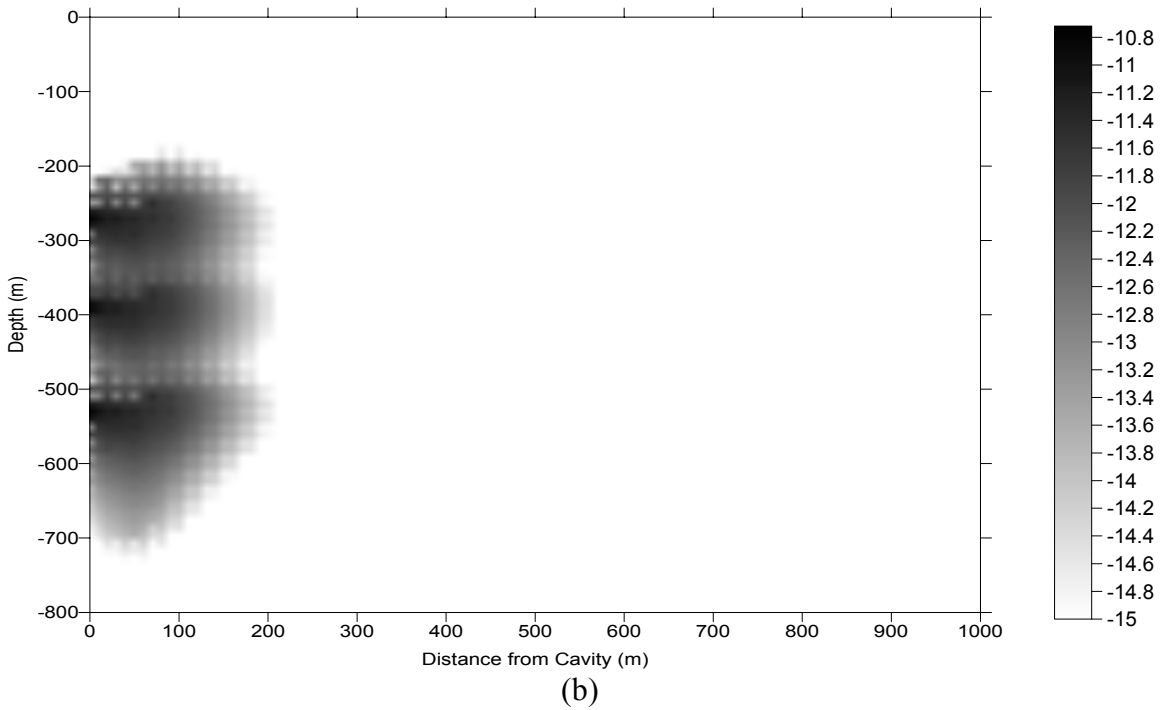
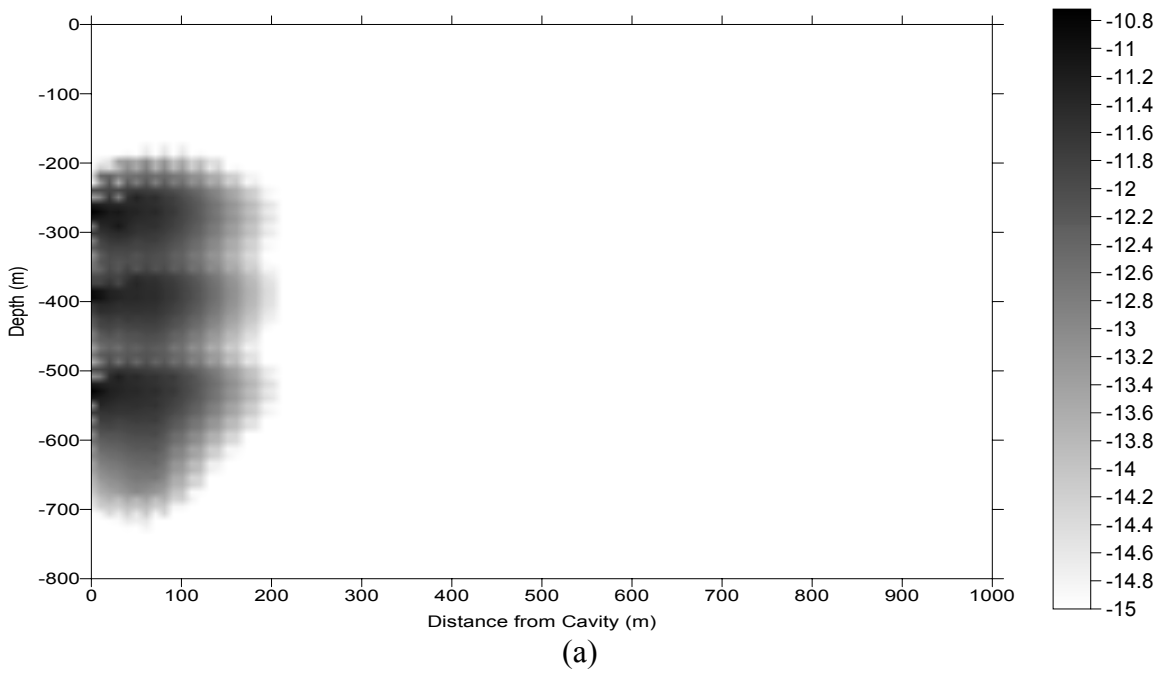
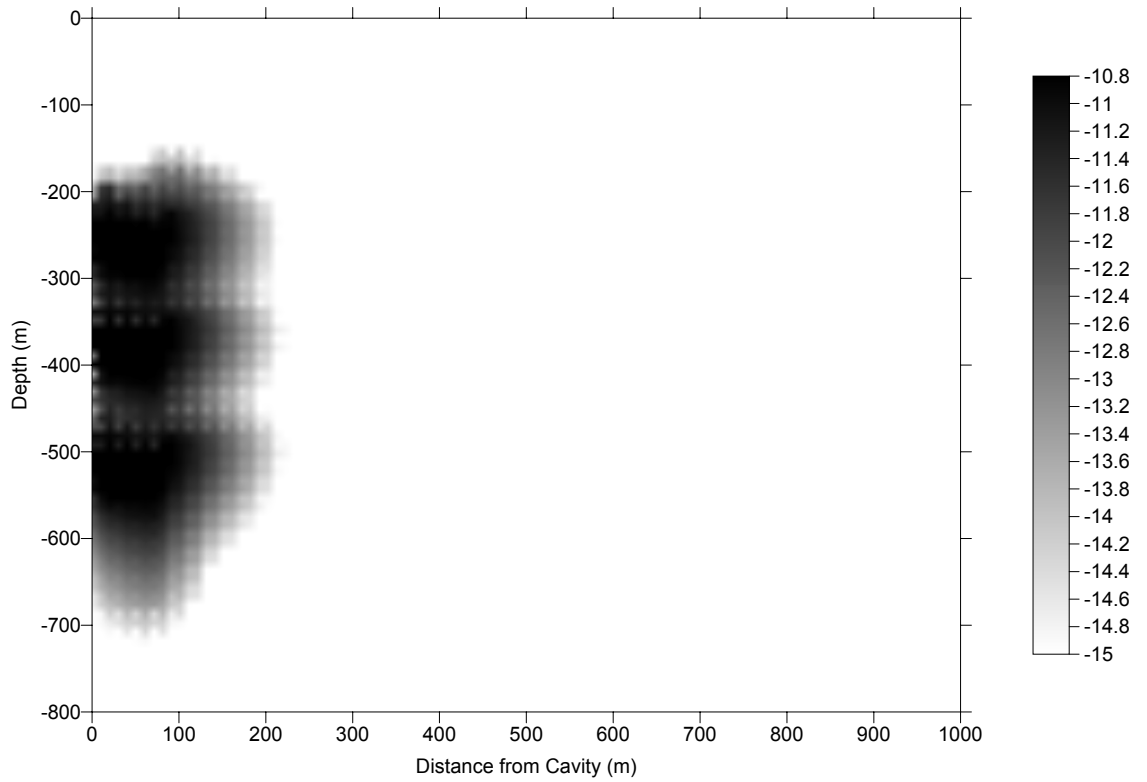
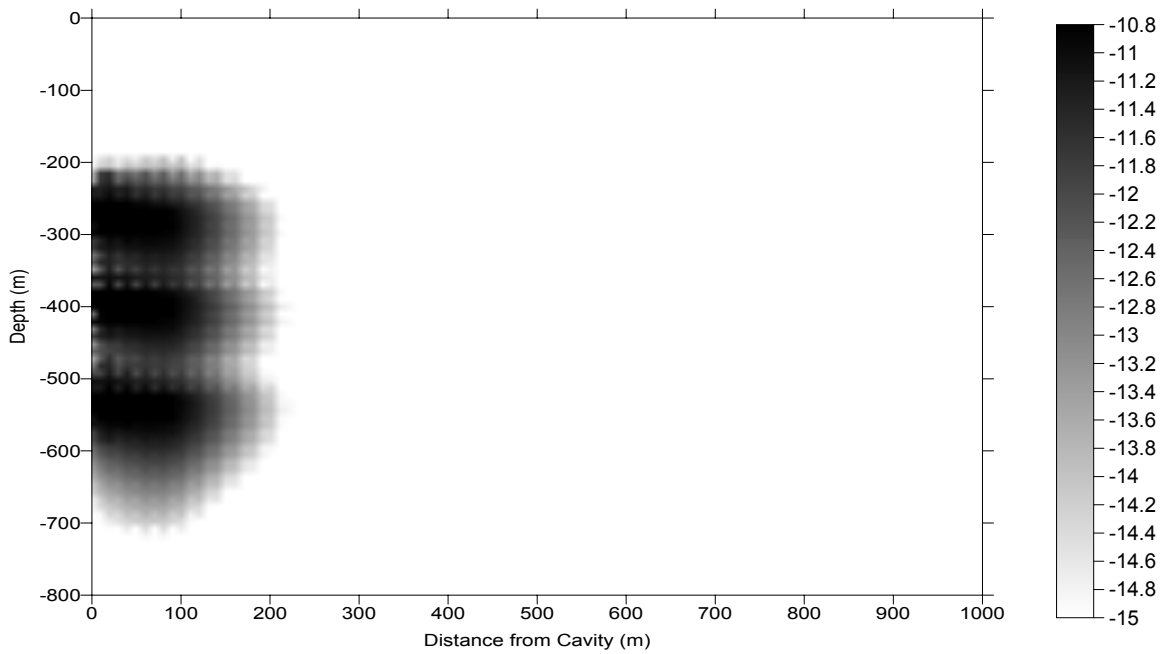


Figure 14. Fracture and matrix simulations at (a) and (b) 50 years and (c) and (d) 100 years for dual permeability simulations.



(c)



(d)

Figure 14. Fracture and matrix simulations at (a) and (b) 50 years and (c) and (d) 100 years for dual permeability simulations (continued).

was inputted as 0.01, which is an order of magnitude smaller than the matrix porosity. The result is higher velocity gas flow through the fractures than through the matrix.

The results show qualitatively different behavior than any of the other simulations. Fracture flow within 80 m of the borehole allows tritium to be transported farther in a shorter time than for any of the porous media simulations. This essentially short circuits flow in the near-field matrix and results in a large tritium concentration gradient at 80 m, instead of the large gradient at the cavity/chimney boundary. However, past 80 m, flow is entirely through the matrix and has similar characteristics to the porous media simulations.

Incorporation of fractures in this manner allows the full effect of matrix diffusion to be present. That is, as flow passes through a fracture, a concentration gradient of tritium develops from the fracture to the matrix because most of the flow through the fracture is gas with radionuclides. Ambient gas in the matrix does not contain radionuclides from the detonations, since both gas and liquid flow is much slower through the matrix. The effect is that some of the radionuclides become stored in the matrix, where they are relatively immobile. As the radionuclides reside in the matrix, they undergo decay to inert helium gas.

Numerous possibilities exist to study the effects of fracture properties on flow and transport in the near field between 0 and 80 m from the boundary. In Figure 14, it was assumed that the matrix and fracture permeability are equivalent; however, this need not be the case. A thorough sensitivity study would look at horizontal and vertical fracture spacing, permeability, the number of subcontinua (*i.e.*, the number of concentric squares consisting of matrix located between fractures) required for accurate simulation, fracture porosity, fracture orientation, and different capillary pressure and relative permeability curves. This is where much of the challenge lies for accurate simulation of the three nuclear-stimulation sites.

6.0 DISCUSSION

6.1 Observations Specific to Rio Blanco

Based upon the input data and assumptions, these preliminary simulation results suggest that radionuclides may be contained within several hundred m of the outer edge of the cavity/chimney. These simulations are very preliminary: they probably capture most of the large-scale features of the flow but may miss some small-scale effects. Further investigation is required to determine the importance of small-scale effects on the overall transport behavior.

Transport of tritium is primarily horizontal and downward -- there are no buoyancy effects. Depending upon the near-field permeability distribution, there may or may not be vertical mixing between the three source locations. The pressure field establishes a steady state within approximately 30 years, at which time tritium has reached its maximum extent. Further extent past this time is balanced by radioactive decay. A one order-of-magnitude increase in permeability results in a travel distance of approximately two times; that is, the concentration field extends to approximately 500 m when k is increased from $3 \times 10^{-17} \text{ m}^2$ to $3 \times 10^{-16} \text{ m}^2$.

The initial fracture simulations show that the problem can be correctly formulated using the MINC module embodied in TOUGH2. The MINC module attempts to model fractures discretely, as opposed to an effective parameterization scheme. However, more simulations are required using the MINC module to grasp the bounds of certainty. Aspects of fracture flow as they pertain to all three gas-stimulation sites are discussed below. was inputted as 0.01, which is an order of magnitude smaller than the matrix porosity. The result is higher velocity gas flow through the fractures than through the matrix.

The results show qualitatively different behavior than any of the other simulations. Fracture flow within 80 m of the borehole allows tritium to be transported farther in a shorter time than for any of the porous media simulations. This essentially short circuits flow in the near-field matrix and results in a large tritium concentration gradient at 80 m, instead of the large gradient at the cavity/chimney boundary. However, past 80 m, flow is entirely through the matrix and has similar characteristics to the porous media simulations.

Incorporation of fractures in this manner allows the full effect of matrix diffusion to be present. That is, as flow passes through a fracture, a concentration gradient of tritium develops from the fracture to the matrix because most of the flow through the fracture is gas with radionuclides. Ambient gas in the matrix does not contain radionuclides from the detonations, since both gas and liquid flow is much slower through the matrix. The effect is that some of the radionuclides become stored in the matrix, where they are relatively immobile. As the radionuclides reside in the matrix, they undergo decay to inert helium gas.

Numerous possibilities exist to study the effects of fracture properties on flow and transport in the near field between 0 and 80 m from the boundary. In Figure 14, it was assumed that the matrix and fracture permeability are equivalent; however, this need not be the case. A thorough sensitivity study would look at horizontal and vertical fracture spacing, permeability, the number of subcontinua (*i.e.*, the number of concentric squares consisting of matrix located between fractures) required for accurate simulation, fracture porosity, fracture orientation, and different capillary pressure and relative permeability curves. This is where much of the challenge lies for accurate simulation of the three nuclear-stimulation sites.

6.0 DISCUSSION

6.1 Observations Specific to Rio Blanco

Based upon the input data and assumptions, these preliminary simulation results suggest that radionuclides may be contained within several hundred m of the outer edge of the cavity/chimney. These simulations are very preliminary: they probably capture most of the large-scale features of the flow but may miss some small-scale effects. Further investigation is required to determine the importance of small-scale effects on the overall transport behavior.

Transport of tritium is primarily horizontal and downward -- there are no buoyancy effects. Depending upon the near-field permeability distribution, there may or may not be vertical mixing between the three source locations. The pressure field establishes a steady state within approximately 30 years, at which time tritium has reached its maximum extent. Further extent past this time is balanced by radioactive decay. A one order-of-magnitude increase in permeability results in a travel distance of approximately two times; that is, the concentration field extends to approximately 500 m when k is increased from $3 \times 10^{-17} \text{ m}^2$ to $3 \times 10^{-16} \text{ m}^2$.

The initial fracture simulations show that the problem can be correctly formulated using the MINC module embodied in TOUGH2. The MINC module attempts to model fractures discretely, as opposed to an effective parameterization scheme. However, more simulations are required using the MINC module to grasp the bounds of certainty. Aspects of fracture flow as they pertain to all three gas-stimulation sites are discussed below.

Although the post-test pressure field history is not known very well, its effect is easily captured in bounding calculations once a refined model is developed.

6.2 General Observations Pertinent to all Sites

Probably the largest limitation to accurate simulation of gas and liquid transport at the three gas-stimulation sites is the absence of a good fracture model. There are actually two aspects to this. The first is that there is not a clear understanding of the spatial distribution of fractures around a test, including their hydraulic properties, geometry, connectivity, and spatial distribution. The second is that there is little knowledge of multiphase flow through fractures; that is, in addition to the absence of a correct model, there is a large gap in understanding of the two-phase flow physics that occur in natural rock fractures and fracture networks. Hence a large degree of uncertainty must be accepted for models that include flow and transport through fractures and fracture networks.

In saturated (*i.e.*, single-phase) studies of flow through fractured media, it is common to assume that flow through fractures is similar to that through porous media, with an enhanced permeability. This same approach is used here in the heterogeneous porous media simulations to acquire a grasp of the region of contamination. However, in addition to viscous and gravity forces that occur in single-phase flow, two-phase flow through fractures includes capillary forces. These can be very important because they alter the pressure (often over orders of magnitude) for which various saturation values exist. Capillary forces also affect the shape of the relative permeability curve, and therefore the relationship between flow (and transport) and the total pressure gradient.

There appears to be no class of capillary pressure or relative permeability functions appropriate for multiphase flow through fractures. These are required for any model that includes flow discretely through fractures. The MINC approach used here assumed that the hydraulic properties of the fractures are the same as for the matrix. This is a good first order approximation, but probably breaks down when small-scale effects are examined.

A second approach to modeling two-phase flow through fractures is to model the fracture/matrix medium as an effective continuum. That is, flow is computed through an equivalent fracture and through the matrix, and then a weighted average of the two is used. It is not clear if this effect method would account for matrix diffusion, however, as the fractures are not modeled discretely. Clearly, some code enhancements are required for this method to be implemented. The effective continuum model has been successfully implemented in an earlier version of TOUGH (Pruess, 1988; Cooper, 1990), although it was exclusively for flow (no transport was included).

A second major limitation in the accurate depiction of flow and transport around nuclear-stimulation sites is the lack of an accurate initial condition. Little is known about the distribution of radionuclides and their properties, in addition to the in-situ fluid, around the test locations at the three nuclear-stimulation sites. As the temperature increased to thousands of degrees centigrade, the fluids passed from a sub- to super-critical state, and then back again to a sub-critical state as the formation cooled. Models exist for the cavity/chimney dimensions, but the degree of mixing of radionuclides in the initial months and years following a detonation is not known. Better near-field models are required that explain behavior in the months following a detonation to set up the initial condition for these types of simulations. The nonisothermal simulations suggest that temperature perturbations on the order of 50°C above ambient, together with a “typical” geothermal gradient, have little effect on the transport field. This needs to be carefully checked as more accurate models of transport are assembled.

7.0 CONCLUSIONS

The correct simulation of radionuclide transport in fractured gas reservoirs hinges upon an accurate model of two-phase flow through fractures. These preliminary simulations suggest the geometry of the large-scale feature of the flow and transport field, but have ignored many small-scale effects. Incorporation of fractures discretely as done here (using the MINC module) should be compared with other fracture models, such as an effective continuum approach. A thorough uncertainty analysis is required to bound the flow and transport calculations as a function of the variables in the fracture model. A Monte Carlo approach could be implemented that includes both discrete fracture properties and intrinsic permeability to capture the bounds on flow and transport.

Radionuclide migration in fractured gas reservoirs is a challenging problem as flow and transport occur within two phases, subject to gravitational, viscous, and capillary effects. In addition, there are phase changes, and interactions between the fractures and matrix, that occur to retard transport. The TOUGH2 simulator is an ideal tool for simulating flow and transport through these sites, as most of the effects are easily implemented into the simulator. In addition, the code is very flexible, and the source code is available so that user-specified modifications can be implemented.

8.0 REFERENCES

- Bear, J., 1988. *Dynamics of Fluids in Porous Media*, Dover reprint of original Elsevier (1972) publication, 764pp.
- Beaver, D.W., 1972. Gas Flow to Multiple Chimneys, Appendix I, in Toman and Tewes, Project Rio Blanco: Phase I Technical Studies, UCID-15968, Lawrence Livermore National Laboratory, pp. 75-106.
- Borg, I.Y., R. Stone, H.B. Levy and L.D. Ramspott, 1976. Information pertinent to the migration of radionuclides in ground water at the Nevada Test Site, UCRL-52078 pt. 1, Lawrence Livermore National Laboratory.
- CER Geonuclear Corporation, date unknown. Project Rio Blanco Reservoir Report, PNE-RB-3.
- Cooper, C.A., 1990. Numerical simulation of gas flow through unsaturated fractured rock at Yucca Mountain, Nevada, Masters Thesis, University of Nevada, Reno, 81 pp.
- Corey, A.T., 1954. The interrelation between gas and oil relative permeabilities, *Producers Monthly*, V. XIX, no. 1, pp. 38-44, November.
- Corey, A.T., 1994. *Mechanics of Immiscible Fluids in Porous Media*, Water Resources Publications, third edition, 252 pp.
- Cussler, E.L., 1997. *Diffusion Mass Transfer in Fluid Systems*, 2nd edition, Cambridge University Press, 580 pp.
- Faure, G., 1977. *Principles of Isotope Geology*, Wiley, 464 pp.
- Hansley, P.L. and R.C. Johnson, 1980. Mineralogy and diagenesis of low-permeability sandstones of Late Cretaceous age, Piceance Creek Basin, Northwestern Colorado, *The Mountain Geologist*, v. 17, no. 4, p. 88-129.
- Johnson, R.C., 1989. Geologic History and Hydrocarbon Potential of Late Cretaceous-Age, Low-Permeability Reservoirs, Piceance Basin, Western Colorado, Chapter E. of Evolution of Sedimentary Basins – Uinta and Piceance Basins, U.S. Geological Survey Bulletin 1787, E1-E51.

- Knutson, C.F., 1975. *Project Rio Blanco summary of related hydrology program to September 1974*, CER Geonuclear Corporation, Las Vegas, Nevada.
- Lorenz, J.C., L.W. Teufel, and N.R. Warpinski, 1991. Regional Fractures I: A mechanism for the formation of regional fractures at depth in flat-lying reservoirs, *Amer. Assoc. Petrol. Geol. Bull.*, v. 75, no. 11, pp. 1714-1737.
- Lorenz, J.C. and S.J. Finley, 1991. Regional Fractures II: Fracturing of Mesaverde reservoirs in the Piceance Basin, Colorado, *Amer. Assoc. Petrol. Geol. Bull.*, v. 75, no. 11, pp. 1738-1757.
- McKee, C.R. and M.E. Hanson, 1975. Explosively created permeability from single charges, *Soc. Petrol. Eng. J.*, v. 15, pp. 495-501.
- Mills, R., 1973. Self-diffusion in normal and heavy water in the range 1-45°, *J. of Physical Chem.*, v. 77, no. 5, pp. 685-688.
- Pitman, J.K. and E.S. Sprunt, 1986. Origin and distribution of fractures in Lower Tertiary and Upper Cretaceous rocks, Piceance Basin, Colorado, and their relation to the occurrence of hydrocarbons, *American Association of Petroleum Geologists Studies in Geology* 24, p. 221-234.
- Pitman, J.K., C.W. Spencer and R.M. Pollastro, 1989. Petrography, mineralogy, and reservoir characteristics of the upper cretaceous Mesaverde Group in the East-Central Piceance Basin, Colorado, Chapter G in *Evolution of Sedimentary Basins – Uinta and Piceance Basins*, U.S. Geological Survey Bulletin, 31 pp.
- Pruess, K. and T.N. Narasimhan, 1985. A practical method for modeling fluid and heat flow in fractured porous media, *Soc. Pet. Eng. J.*, v. 25, no. 1, pp. 14-26.
- Pruess, K., 1987. TOUGH User's Guide, Rpt. LBL-20700, 78 pp., Lawrence Berkeley Laboratory.
- Pruess, K., J.S.Y. Wang and Y.W. Tsang, 1988. Effective continuum approximation for modeling fluid and heat flow in fractured porous tuff, Rpt. SAND-7000, Sandia National Laboratories, Albuquerque, New Mexico, 99 pp.
- Pruess, K., C. Oldenburg and G. Moridis, 1999, *TOUGH2 User's Guide, Version 2.0*, LBNL-43134, Berkeley, California.
- Reid, R.C., J.M. Prausnitz and B.E. Poling, 1987. *The Properties of Gases and Liquids*, McGraw Hill, 741 pp.
- Rocky Mountain Map Co., 1999. Structure Contour Map of N ½ Piceance Basin, Douglas Creek Arch, Colorado; Casper, Wyoming.
- Takahashi, S., 1974. *J. Chem. Eng. Japan*, v. 7, p. 417.
- Taylor, R.W., 1972. Divining gas pressure at Rio Blanco, Appendix H, in Toman and Tewes, *Project Rio Blanco: Phase I Technical Studies*, UCID-15968, Lawrence Livermore National Laboratory, pp. 62-74.
- Toman, J., 1975. Production test data and preliminary analysis of top chimney/cavity, *Nuclear Technology*, v. 27, pp. 692-704.
- Toman, J. and H.A. Tewes, 1972. *Project Rio Blanco: Phase I technical studies*, UCID-15968, Lawrence Livermore Laboratory, 138 pp.
- U.S. Department of Energy, 2000. *United States Nuclear Tests. July 1945 through September 1992*, DOE/NV--209.

- U.S. Energy Research and Development Administration and Continental Oil Company, 1975. Project Rio Blanco Data Report: Production testing alternate reentry hole RB-AR-2, NVO-154.
- U.S. Environmental Protection Agency, 1992. Offsite Environmental Monitoring Report: Radiation Monitoring Around United States Nuclear Test Areas, Calendar Year 1991, EPA 600/R-93/141.
- Wang, J.S.Y. and T.N. Narasimhan, 1985. Hydrologic mechanisms governing fluid flow in a partially saturated, fractured, porous medium, *Water Resour. Res.*, v. 21, pp. 1861-1874.
- Warren J.E. and P.J. Root, 1963. The behavior of naturally fractured reservoirs, *Soc. Petrol. Eng. J.*, v. 228, pp. 245-255.
- Wu, Y-S. and K. Pruess, 2000. Numerical simulation of non-isothermal multiphase tracer transport in heterogeneous fractured porous media, *Advances in Water Resources*, v. 23, pp. 699-723.